Polypharmacological Profile of 1,2-Dihydro-2-Oxo-Pyridine-3-Carboxamides in the Endocannabinoid System

Andrea Chicca,[b,1] Chiara Arena,[a,1] Simone Bertini,[a] Francesca Gado,[a] Elena Ciaglia,[d] Mario Abate,[d] Maria Digiacomo,[a] Margherita Lapillo,[a] Giulio Poli,[e] Maurizio Bifulco,[c] Marco Macchia,[a] Tiziano Tuccinardi,[a,f] Jürg Gertsch,[b] Clementina Manera[a,*]

[a] Department of Pharmacy, University of Pisa, 56126 Pisa. [b] Institute of Biochemistry and Molecular Medicine, NCCR TransCure, University of Bern, Bühlstrasse 28, CH-3012 Bern, Switzerland. [c] Department of Molecular Medicine and Medical Biotechnology, University of Naples Federico II, 80131 Naples, Italy. [d] Department of Medicine, Surgery and Dentistry "Scuola Medica Salernitana", University of Salerno, 84081 Baronissi, Salerno, Italy [e] Department of Biotechnology, Chemistry and Pharmacy, University of Siena, via Aldo Moro 2, 53019 Siena, Italy; [g]Sbarro Institute for Cancer Research and Molecular Medicine, Center for Biotechnology, College of Science and Technology, Temple University, Philadelphia, PA, USA.

Corresponding Author
*Clementina Manera: Phone: +39 050 2219548. Fax: +39 050 2210680. e-mail: clementina.manera@farm.unipi.it.
ORCID
Clementina Manera: 0000-0002-7379-5743

[1]Author Contributions
A. C. and C. A. contributed equally.

Notes
The authors declare no competing financial interest.

RECEIVED DATE (to be automatically inserted after your manuscript is accepted if required according to the journal that you are submitting your paper to)

Highlights

- We synthesized 1,2-dihydropyridine-2-oxo-3-carboxamide with multi-activity on ECS
- Some derivatives showed cytotoxic activity on U937 lymphoblastoid cell
- Molecular docking on 3D structures of CBRs and of FAAH suggested their binding mode

Graphical abstract

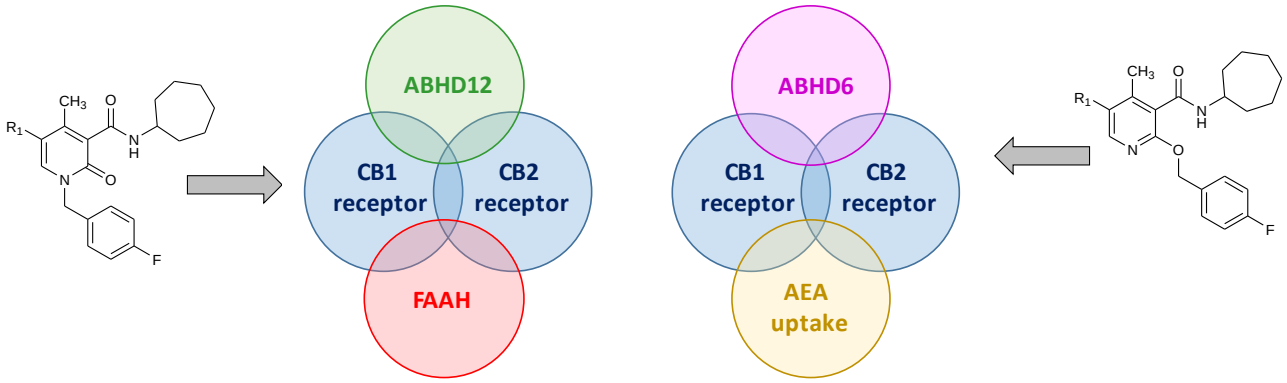

ABSTRACT

The endocannabinoid system (ECS) represents one of the major neuromodulatory systems involved in different physiological and pathological processes. Multi-target compounds exert their activities by acting via multiple mechanisms of action and represent a promising pharmacological modulation of the ECS. In this work we report 4-substituted and 4,5-disubstituted 1,2-dihydro-2-oxo-pyridine-3-carboxamide derivatives with a broad spectrum of affinity and functional activity towards both cannabinoid receptors and additional effects on the main components of the ECS. In particular compound **B3** showed high affinity for CB1R (K_i = 23.1 nM, partial agonist) and CB2R (K_i = 6.9 nM, inverse agonist) and also significant inhibitory activity (IC_{50} = 70 nM) on FAAH with moderate inhibition of ABHD12 (IC_{50} = 2.5 μM). Compounds **B4**, **B5** and **B6** that act as full agonists at CB1R and as partial agonists (**B5** and **B6**) or antagonist (**B4**) at CB2R, exhibited an additional multi-target property by inhibiting anandamide uptake with sub-micromolar IC_{50} values (0.28–0.62 μM). The best derivatives showed cytotoxic activity on U937 lymphoblastoid cells. Finally, molecular docking analysis carried out on the three-dimensional structures of CB1R and CB2R and of FAAH allowed to rationalize the structure-activity relationships of this series of compounds.

Keywords: Endocannabinoid system; Cannabinoid receptors; Polypharmacology; Molecular docking; U251MG glioblastoma cell line; U937 lymphoblastoid cells;

1. Introduction

The endocannabinoid system (ECS) consists of two G protein-coupled receptors, the type-1 (CB1R) and type-2 (CB2R) cannabinoid receptor, a class of lipids mediators called endocannabinoids (ECs) which are produced on-demand from membrane phospholipid precursors and several enzymes involved in the biosynthesis and degradation of ECs. So far, the most well-studied ECs are *N*-arachidonoylethanolamine (anandamide, AEA), which is a member of the large family of *N*-acylethanolamines (NAEs) and 2-arachidonoylglycerol (2-AG) that belongs to the monoacylglycerol family [1]. The biological activities of these lipid mediators are terminated upon cellular re-uptake and subsequent metabolism. The main endocannabinoid degrading enzymes are fatty acid amide hydrolase (FAAH) [2] for AEA and monoacylglycerol lipase (MAGL) [3] for 2-AG. Two serine hydrolases α,β-hydrolase domain-6 (ABHD6) and α,β-hydrolase domain-12 (ABHD12) were recently identified as complementary 2-AG-degrading enzymes in the brain [4,5].

The ECS is involved in different physiological and pathological processes including cancer, appetite, memory, neuropathic and inflammatory pain, obesity, neuroprotection and neurodegenerative diseases [6]. Numerous CB1R and CB2R ligands have been developed and tested in vitro and in vivo in the context of drug discovery, but none of them reached an advanced stage of clinical development due to central or peripheral side effects that are mainly associated to chronic activation or blocking of CB1R [7-9]. Alternative strategies to modulate the ECS are focused on the increase of AEA and 2-AG levels by inhibiting their enzymatic degradation thus preserving the beneficial effects derived from the direct activation of cannabinoid receptors (CBRs) by their endogenous ligands [10]. These efforts led to the generation of many potent and selective inhibitors of the main enzymes involved in AEA and 2-AG metabolism (FAAH, MAGL, ABHDs) [11-13]. However in preclinical animal models, the repeated administrations of covalent MAGL inhibitors rapidly induced CB1R desensitization in the brain [14], while chronic ablation of FAAH

activity may be associated to potential side effects on the cardiovascular and metabolic system [15,16].

Recent findings highlighted the emerging role of each target of the ECS to control symptoms and progression of several diseases [17,18]. Multi-target compounds exert pro-cannabinoid activities by means of more than one mechanism of action [19]. Indeed, it is reasonable to assume that the simultaneous modulation of more targets within the ECS may offer a safer and more effective pharmacological strategy to tackle the complexity of the ECS [19]. However, a proper evaluation of the different multi-target approaches as compared to the classic modulation of a single target needs to be further investigated. Therefore, the development of different multi-target compounds could get a foothold to better explore the polypharmacology of the ECS and to assess its potential pharmacological advantages for the treatment of different pathologies.

Previously, in a research program aimed at obtaining CB2R selective ligands [20-23], a series of 1,2-dihydro-2-oxo-pyridine-3-carboxamide derivatives with general structure **A**, (Figure 1) was developed [24,25].

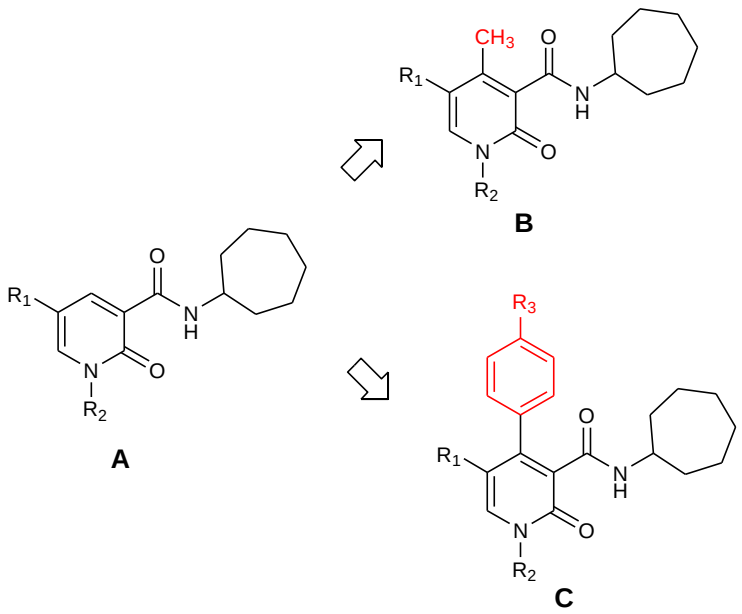

Figure 1. General structure of 1,2-dihydro-2-oxo-pyridine-3-carboxamide derivatives **A**, **B** and **C**.

These compounds showed a broad spectrum of affinity for both CB1R and CB2R. Furthermore, the functional activity of this series is controlled by the presence of a substituent at the position 5 of the 2-oxo-pyridine nucleus [25]. The significant affinity and selectivity towards CB2R displayed by some derivatives of **A** make this new scaffold useful as initial building block for designing new CB2R ligands. For this reason and to further investigate the structure-activity relationships (SAR) of this series of compounds, in this study the central scaffold **A** was modified by insertion of a methyl group (**B1-B4**, Figure 1) or an aryl moiety (compounds **C1-C6**, Figure 1) at the 4-position of the 1,2-dihydro-2-oxo-pyridine ring to obtain 4-substituted or 4,5-disubstituted-1,2-dihydro-2-oxo-pyridine-3-carboxamide derivatives (Table 1). The new compounds are characterized by the presence of a *p*-fluorobenzyl moiety at the N-1 position of the 1,2-dihydro-2-oxo-pyridine ring (R1) and a *N*-cycloheptyl carboxamide group at the 3-position that were chosen on the basis of the best results obtained with the previous series. Furthermore, the substituent in the N-1 position was shifted to the oxygen in position 2 of the heterocyclic nucleus (**B5** and **B6**, Table 1).

The new 1,2-dihydro-2-oxo-pyridine-3-carboxamide derivatives **B** and **C** were evaluated for their binding affinities (K_i values) for both CB1R and CB2R. Subsequently, the compounds which showed the most potent CBRs affinity values were also investigated for their functional activity using a [^{35}S]GTPγS assay. All the synthesized compounds were tested on the main targets of the ECS (MAGL, FAAH, ABHDs and AEA cellular uptake). The best compounds were also tested for their capability to inhibit viability of U251MG glioblastoma cell line and that of U937 lymphoblastoid cells. Finally, to rationalize the experimentally observed SAR, a molecular docking analysis of the synthetized compounds was carried out into the three-dimensional structure of CB1R and CB2R and of FAAH.

2. Results and discussion

2.1 Chemistry

The synthesis of 1,2-dihydro-2-oxopyridine derivatives **B1-B4** and **C1-C6** and 2-substituted pyridines **B5** and **B6** was accomplished as depicted in Schemes 1-4. As reported in Scheme 1, 1,2-dihydro-4-methyl-2-oxo-pyridine-3-carbonitrile (**1**) synthesized as reported in literature [21] from 4,4-dimethoxyl-2-butanone with cyanoacetamide, was hydrolyzed to the corresponding carboxylic acid derivative **2** by heating at 120 °C with 50% H_2SO_4 (w/v). Treatment of **2** with concentrated H_2SO_4 in MeOH, carried out under microwave irradiation at 100 °C for 50 minutes or under conventional heating at 85 °C for 12 h, gave the corresponding methyl ester **3**. The treatment of **3** with cycloheptylamine under microwave irradiation at 130 °C for 30 minutes or under conventional heating at 150 °C for 48 h provided the carboxamide derivative **4**. Finally, compound **4** was treated with CsF in anhydrous DMF and then with *p*-fluorobenzyl chloride to afford the desired *N*-alkylated derivative **B1** together to the *O*-substituted derivative **B5**, analogously to previously reported for compounds **A** [24,25]. The two structural isomers were purified by flash chromatography.

Scheme 1. Synthesis of the 1,2-dihydro-4-methyl-2-oxo-pyridine **B1** and 2-substituted pyridine **B5**.

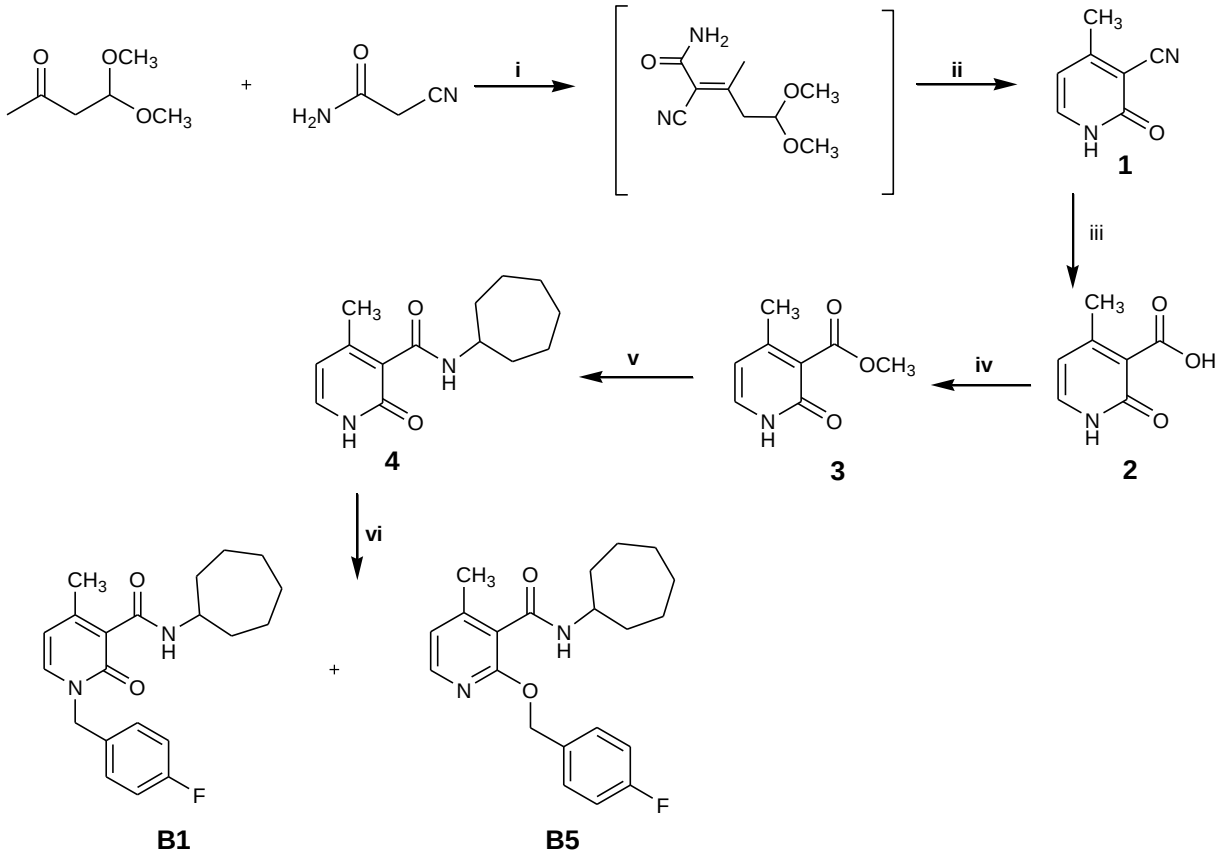

Reagents and conditions: (i) NH_4OAc, AcOH, toluene, 116 °C, 8 h; (ii) conc. H_2SO_4, 50 °C, 3 h; (iii) 50% H_2SO_4, 120 °C, 8 h; (iv) MeOH, conc. H_2SO_4., MW, 110 °C, 50 min, (200 W, 100 psi) or 85 °C, 12 h; (v) cycloheptylamine, MW, 130 °C, 30 min, (140 W, 100 psi) or 150 °C, 48 h; (vi) 1) CsF, dry DMF, rt, 1 h; 2) *p*-fluorobenzyl chloride, rt, 12 h.

The synthesis of the 4,5-disubstituted derivatives **B2-B4** and **B6** was carried out starting from compound **4** (Scheme 2), which was treated with a solution of bromine in $CHCl_3$ affording the corresponding 5-bromo derivative **5**. The desired *N*-alkylated derivative **B2** was obtained by treatment of **5** with *p*-fluorobenzyl chloride *via* a procedure similar to that previously used for compound **B1**. Also in this case, the *O*-substituted derivative **B6** was obtained. The 5-aryl derivatives **B3** and **B4** were obtained starting from the 5-bromo derivative **B2** *via* a Suzuki cross-

coupling reaction with the suitable boronic acids in dry toluene by generating *in situ* $Pd(PPh_3)_4$ as the catalyst and with anhydrous potassium carbonate as the base, refluxing at 100 °C, for 12 h.

Scheme 2. Synthesis of 4-methyl-1,2-dihydro-2-oxo-pyridine **B2-B4** and 2-substituted pyridine **B6**.

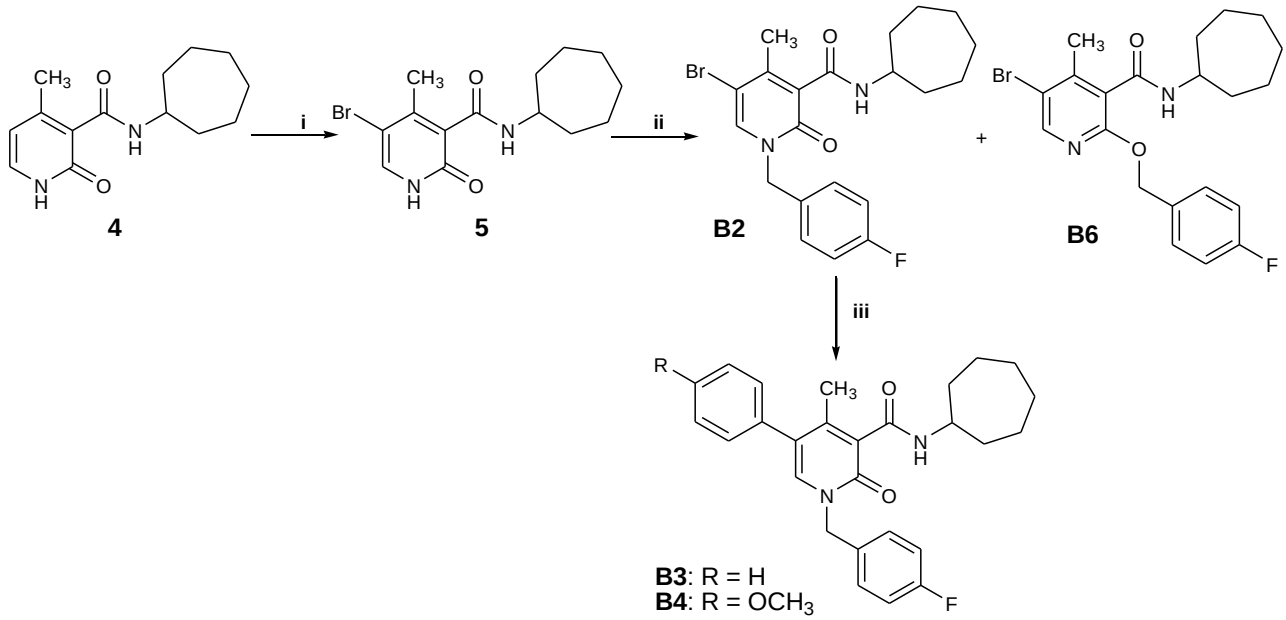

Reagents and conditions: (i) Br_2, $CHCl_3$, rt, 12 h; (ii) anhydrous DMF, CsF, rt, 1 h, p-fluorobenzyl chloride, rt, 12 h; (iii) 1) anhydrous toluene, PPh_3, $Pd(OAc)_2$, rt, 15 min; 2) K_2CO_3, suitable arylboronic acid, 100 °C, 12 h.

Initially, the synthesis of 4-aryl substituted compounds **C1-C6** (Table 1) was planned as described in Scheme 3, starting from acetophenone or *p*-methoxyacetophenone which by Knoevenagel condensation with ethyl cyanoacetate afforded the ethyl 2-cyano-3-arylbut-2-enoate derivatives **6** or **7** respectively [27]. The reaction of compounds **6** or **7** with dimethylformamide-dimethylacetal (DMF-DMA), at room temperature gave the enaminonitriles **8** and **9**, respectively [27]. Finally, the cyclization of the enaminonitriles **8** or **9** with *p*-flurobenzylamine, at 90 °C led to the desired 3-cyano-2-pyridones **10** or **11** (see Supporting Information for experimental details).

Unfortunately, several attempts made to hydrolyze the 3-cyano-2-pyridones to the corresponding carboxylic acid derivatives have not been successful.

Scheme 3. Attempt for the synthesis of 4-aryl-1,2-dihydro-2-oxo-pyridine.

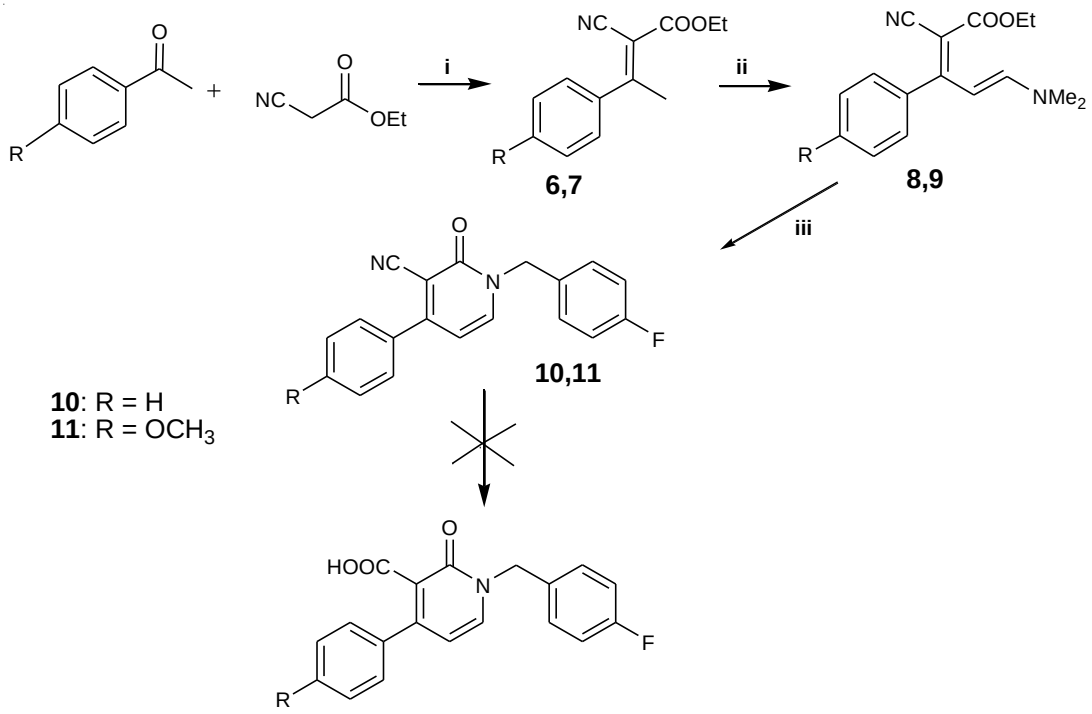

Reagents and conditions: (i) $TiCl_4$, pyridine, CH_2Cl_2, 0 °C to rt., 12 h; (ii) DMF-DMA, solvent-free, 24 h; (iii) *p*-fluorobenzylamine, solvent-free, 90 °C, 2 h.

For this reason, we focused the attention on a recent procedure to obtain the 2-pyridone scaffold with an aromatic substituent in position 4 [28]. As described in Scheme 4, *N*-alkylation of the commercial available 2-hydroxynicotinic acid with *p*-fluorobenzyl bromide in presence of NaH, followed by hydrolysis with 10% NaOH at reflux and then acidification, afforded the carboxylic acid derivative **12**. The condensation reaction of **12** with cycloheptylamine in presence of TBTU, and *N*,*N*-diisopropylethyl amine (DIPEA), gave the desired carboxamide derivative **13.** Compound **13** was treated with the proper Grignard's reagent (phenylmagnesium bromide or *p*-

methoxyphenylmagnesium bromide) using copper(I) iodide and lithium bromide in dry THF, at -40 °C to obtain the 4-substituted 1,2-dihydro-2-oxo-pyridines **C1** and **C2**. These compounds were then treated with a solution of bromine in $CHCl_3$ to afford the desired compounds **C3** and **C4**. To obtained compounds **C5** and **C6**, derivatives **C3** and **C4** were submitted to a Suzuki cross-coupling reaction with the suitable arylboronic acid, in dry toluene by generating *in situ* $Pd(PPh_3)_4$ as the catalyst and with anhydrous potassium carbonate as the base, refluxing at 100 °C.

Scheme 4. Synthesis of 4-aryl-1,2-dihydro-2-oxo-pyridines **C1-C6**.

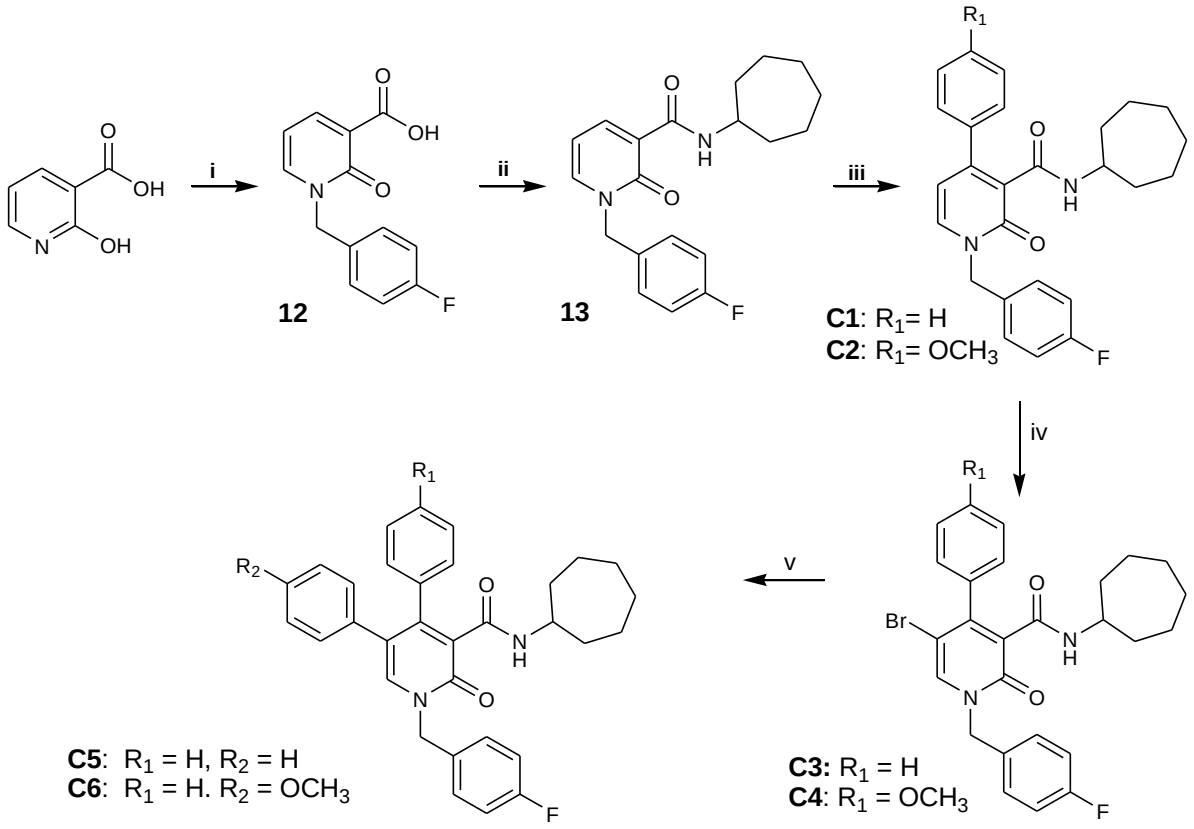

Reagents and conditions: (i) 1) NaH, *p*-fluorobenzyl bromide, dry DMF, 50 °C, 12 h; 2) 10% NaOH, reflux, 100 °C, 4 h; (ii) 1) anhydrous DMF, DIPEA, TBTU, 0 °C, 30 min, 2) cycloheptylamine, 0 °C to rt, 12 h; (iii) CuI, LiBr, phenylmagnesium bromide or *p*-

methoxyphenylmagnesium bromide, THF, -40 °C, 6 h; (iv) Br_2, $CHCl_3$, rt, 12 h; (v) 1) anhydrous toluene, PPh_3, $Pd(OAc)_2$, rt, 15 min; 2) K_2CO_3, suitable arylboronic acid, 100 °C, 12 h.

2.2. Biological evaluation

2.2.1 CB1R and CB2R affinity

The binding affinities (K_i values) of target compounds were evaluated in competitive radioligand displacement assays against [^{3}H]CP-55,940 using membrane preparations obtained in-house from stable transfected CHO-*h*CB_1 and CHO-*h*CB_2 cells. The results are summarized in Table 1.

Table 1. Data of 1,2-dihydro-2-oxopyridine- and pyridine-3-carboxamide derivatives **B1-B6** and **C1-C6**.[a]

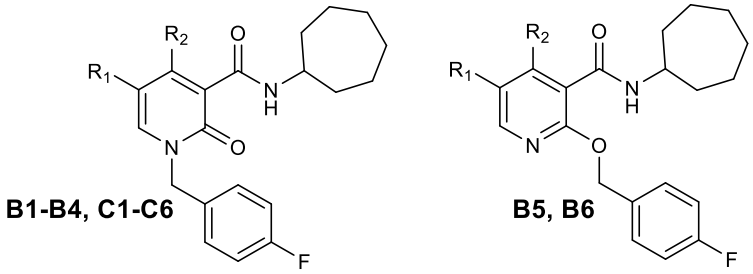

			K_i value (mean ± SD, nM)		IC_{50} (mean ± SD, μM)				
Cmpd	**R1**	**R2**	**CB1R**	**CB2R**	**FAAH**	**MAGL**	**ABHD6**	**ABHD12**	**AEA uptake**
B1	H	CH_3	11.7 ± 3.6	5.9 ± 1.5	8.8 ± 2.6	>10	>10	>10	1.8 ± 0.5

B2	Br	CH_3	2.3 ± 1.6	3.5 ± 4.6)	2.3 ± 0.9	>10	>10	2.1 ± 1.2	0.93 ± 0.33
B3	phenyl	CH_3	23.1 ± 4.2	6.9 ± 3.8	0.07 ± 0.06	>10	>10	2.5 ± 1.1	n.d.
B4	*p*-OCH_3phenyl	CH_3	30.7 ± 9.5	7.9 ± 2.1	1.3 ± 1.1	>10	>10	>10	0.28 ± 0.17
C1	H	Phenyl	>10000	187 ± 65	>10	>10	>10	>10	>10
C2	H	*p*-OCH_3phenyl	>10000	>10000	>10	>10	>10	>10	>10
C3	Br	Phenyl	>10000	437 ± 117	>10	>10	3.0 ± 0.5	>10	>10
C4	Br	*p*-OCH_3phenyl	>10000	>10000	>10	>10	>10	>10	>10
C5	phenyl	Phenyl	>10000	>10000	>10	>10	>10	>10	>10
C6	*p*-OCH_3phenyl	Phenyl	>10000	>10000	>10	>10	>10	>10	>10
B5	H	CH_3	131 ±26	46.3 ± 19.2	>10	>10	>10	>10	0.58 ± 0.19
B6	Br	CH_3	113 ± 63	606 ± 305	>10	>10	0.53 ± 0.21	>10	0.62 ± 0.12

[a]Results are expressed as mean ± SD calculated from at least 3 experiments each performed in triplicate.

The results reported in Table 1 indicate that the pyridine-3-carboxamide derivatives **B1-B6**, **C1** and **C3**, showed nanomolar or submicromolar binding affinities to CB2R and/or CB1R, unlike their analogs **C2** and **C4-C6**. Generally, all ligands tend to show higher affinity for CB2R, with a selectivity factor in the range of 2 to 54. This behavior is in agreement with that previously reported for **A** derivatives [24,25]. The only exceptions were the 5-bromo-4-methyl-derivatives **B2** and **B6** that showed a K_i(CB1R)/K_i(CB2R) ratio of 0.65 and 0.18, respectively. (*R*)-WIN55,212 was used as positive control for both CB1R and CB2R binding experiments and showed K_i value of 2.5 ± 0.9 nM for CB1R and 1.6 ± 0.5 nM for CB2R.

The compounds **B** possess a broad spectrum of affinity towards both CBR subtypes, with K_i values ranging from 2.3 nM (**B2**) to 131 nM (**B5**) for CB1R and from 3.5 nM (**B2**) to 606 nM (**B6**) for CB2R. The results showed that the insertion of a small substituent, like the methyl group at the 4-position of the 1,2-dihydro-2-oxo-pyridine ring (compounds **B1-B4**), does not alter the binding

properties at both CBRs as also shown by the previous reported 5-monosubstituted **A** derivatives [25]. Indeed, these compounds generally showed K_i values in the low nanomolar range (Table 1). On the contrary, the insertion of bulkier substituents, like a phenyl or a *p*-methoxyphenyl group (**C1-C6**), led to a significant decrease of the affinity towards both CBR subtypes independently of the type of substituent at position 5 of the pyridine core. Moreover, when the substituent at the 1-position was shifted to the oxygen at the 2-position of the pyridine ring (compound **B5** and **B6**), the binding affinity for both CBRs decreased by a factor 10 for the 4-methyl-2-substituted derivative **B5** as compared to the corresponding 1-substituted compound **B1**, and by a factor 50 for CB1R and 200 for CB2R in the case of 5-bromo-4-methyl-2-substituted derivative **B6**, as compared to the 5-bromo-4-methyl-1-substituted derivative **B2** (Table 1). These data are in agreement with the results previously reported on the binding affinity of this chemical scaffold [24,25].

Altogether, the results obtained for these new compounds suggest that either the type or the position of the substituent on the pyridine ring play a key role for the binding interactions to the cannabinoid receptors.

2.2.2. CB1R and CB2R functional activity

Compounds that showed the best results in terms of binding properties on CBRs were tested for their functional activity, using the [^{35}S]GTPγS assay. The results are summarized in Table 2 and showed that the new compounds work as full agonists at CB1R, with the exception of **B3** which behaved as partial agonist. Compounds **B1**, **B2**, **B5** and **B6** behaved as partial agonist at CB2R, compound **C3** as full agonist, compounds **B3** and **C1** acted as inverse agonists and compound **B4** as an antagonist. These data indicate that while the combination of substituents in positions 4 and 5 do not modify the agonist behavior at CB1R, they have impacts on CB2R activation. In agreement with what we previously observed with a series of 4-unsubstituted 1,2-dihydro-2-oxo-pyridine-3-carboxamides, the type of substituent in position 5 (R1) dictates the functional behavior at CB2R

generating agonism, antagonism and inverse agonism [25]. The presence of a methyl group in position 4 (R2) combined with a bulky substituent in position 5 leads to antagonism (**B4**) or inverse agonism (**B3**) at CB2R. The increase of the substituent size in position 5 in combination with a phenyl group in position 4 led to a significant loss of CB2R binding activity (H, K_i = 187 nM; Br, K_i = 437 nM; phenyl and *p*-methoxyphenyl, K_i > 10 μM). Interestingly, while the unsubstituted 4-phenyl-derivative (**C1**) behaved as an inverse agonist, the 5-bromo-4-phenyl derivative (**C3**) showed an opposite effect, thus behaving as CB2R full agonist (Table 2). These results suggest that the nature of the substituent in position 5 of the pyridine ring is responsible for the functional switch in accordance to what was previously reported [25], and that the combination with the substituents in position 4 can also play a role in determining the activity of the ligand at CB2R.

CB2R pharmacology is quite versatile and both agonists and inverse agonists showed beneficial effects *in vitro* and *in vivo* [29,30]. CB2Rs have a relatively high ligand-independent (constitutive) activation which makes certain classic receptor antagonists/inverse agonists (e.g. AM630) behaving as agonists and vice versa (e.g. AM1241) depending on the conditions [31,32]. Furthermore, many of the CB2R ligands, including the endocannabinoids AEA and 2-AG behave as functional selective (biased) ligands at CB2R, thus activating only certain signaling pathways, while being inactive or even hindering other pathways [33]. In our experiments we measured the recruitment of G-proteins ([^{35}S]GTPγS assay) as functional assay and compound **B3** and **B4** behaved as inverse agonist and antagonist at CB2R, respectively. Additional studies should be performed to fully characterize the receptor pharmacological profile of this new series of 4-substituted and 4,5-disubstituted-1,2-dihydro-2-oxo-pyridine-3-carboxamide derivatives and may highlight different behaviors at other CB1R- and CB2R-mediated signaling pathways (e.g. cAMP production, β-arrestin, ion channels).

Table 2. Summary of functional activity ([^{35}S]GTPγS assay) of compounds **B1-6** and **C1-6** at CB1R and CB2R. Data are express as mean ± SD obtained from at least three experiments performed in triplicate.

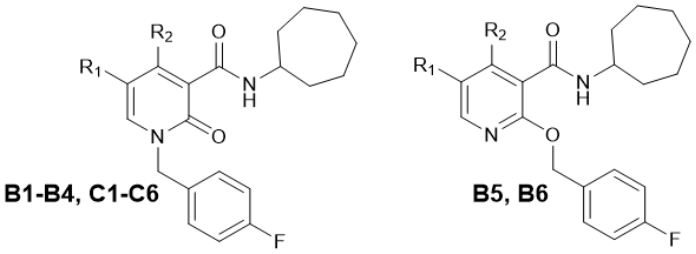

			CB1R		CB2R	
Cmpd	**R1**	**R2**	EC_{50} value (mean ± SD)	Emax (% of control)	EC_{50} value (mean ± SD)	Emax (% of control)
B1	H	CH_3	69 ± 15 nM	227 ± 56 (Full Ago)	1.9 ± 2.5 nM	128 ± 31 (Part Ago)
B2	Br	CH_3	1.4 ± 1.5 nM	198 ± 35 (Full Ago)	1.1 ± 1.8 nM	134 ± 28 (Part Ago)
B3	phenyl	CH_3	237 ± 44 nM	131 ± 42 (Part Ago)	12 ± 10 nM	39 ± 15 (Inv Ago)
B4	*p*-OCH_3phenyl	CH_3	96 ± 38 nM	205 ± 26 (Full Ago)	n.c.	99 ± 6 (Antago)
C1	H	Phenyl	n.d.	n.d.	501 ± 143 nM	134 ± 35 (Part Ago)
C2	H	*p*-OCH_3phenyl	n.d.	n.d.	n.d.	n.d.
C3	Br	Phenyl	n.d.	n.d.	316 ± 96 nM	176 ± 31 (Full Ago)
C4	Br	*p*-OCH_3phenyl	n.d.	n.d.	n.d.	n.d.
C5	phenyl	Phenyl	n.d.	n.d.	n.d.	n.d.
C6	*p*-OCH_3phenyl	Phenyl	n.d.	n.d.	n.d.	n.d.
B5	H	CH_3	229 ± 62 nM	218 ± 28 (Full Ago)	31 ± 20 nM	127 ± 25 (Part Ago)

B6	Br	CH_3	182 ± 51 nM	193 ± 30 (Full Ago)	687 ± 183 nM	125 ± 28 (Part Ago)
CP55940	-	-	5.5 ± 3.9 nM	212 ± 33 (Full Ago)	5.5 ± 3.9 nM	196 ± 21 (Full Ago)
SR1	-	-	36 ± 12 nM	27 ± 19 (Inv Ago)	n.d.	n.d.
AM630	-	-	n.d.	n.d.	167 ± 82 nM	35 ± 12 (Inv Ago)

[a]In brackets the behavior on CB1R and CB2R is reported from the [^{35}S]GTPγS assay: Part Ago: partial agonist; Full Ago: full agonist; Inv Ago: inverse agonist; Antago: antagonist. n.d.: not determined; n.c.: not calculated.

2.2.3. Polypharmacology in the ECS.

In order to further characterize the pharmacology of these new compounds, we tested their effects on the main components of the ECS. Our results identified interesting polypharmacological properties among the tested compounds. The *p*-fluorobenzyl N-1 substituted derivatives bearing a methyl group in position 4 (**B1-B4**) inhibited the main AEA hydrolytic enzyme fatty acid amide hydrolase (FAAH) (Table 1), with increasing potencies in correlation with the presence of a bulkier substituent in position 5. Indeed, while the unsubstituted 4-methyl-deriativative **B1** inhibited FAAH with an IC_{50} value of 8.8 μM, the 4-methyl-5-phenyl derivative **B3** blocked AEA hydrolysis with an IC_{50} value of 70 nM (see Fig. 2). The 4-methyl derivatives where the *p*-fluorobenzyl group was shifted to the oxygen in position 2 of the heterocyclic nucleus (**B5** and **B6**) were completely inactive on FAAH ($IC_{50} > 10$ μM) (Table 1).

In our small compound library, the potency of 1,2-dihydro-2-oxo-pyridine-3-carboxamides to inhibit FAAH was associated with the combined presence of a methyl group in position 4, a bulky substituent in position 5, and the *p*-fluorobenzyl group in the N-1 position of the 1,2-dihydro-2-oxo-pyridine ring (Table 1, Fig. 2).

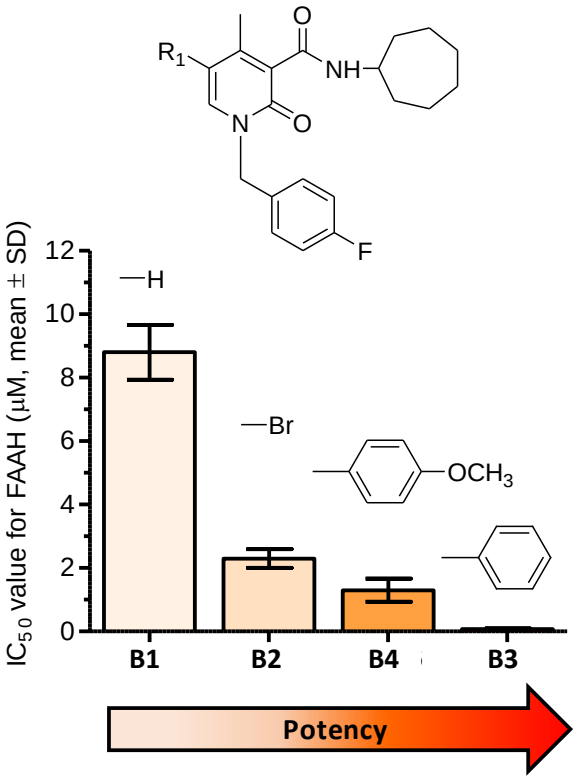

Figure 2. Impact of the substituent in position 5 to the potency for FAAH inhibition.

None of the compounds showed significant effects on the main 2-AG hydrolytic enzyme MAGL, while **B2**, **B3**, **B6**, and **C3** exhibited a moderate low micromolar inhibition of the minor 2-AG hydrolytic enzymes ABDH6 and ABHD12. Compound **C3** selectively inhibited ABHD6 without affecting ABHD12, while **B2** and **B3** inhibited ABHD12 without exerting any effects on ABHD6 up to 10 μM. The 4-methyl-5-bromo derivative **B6** resulted the most potent ABHD6 inhibitor (IC_{50} value of 530 nM). Interestingly, its analog **B2** bearing the *p*-fluorobenzyl substituent at the N-1 position of the 1,2-dihydro-2-oxo-pyridine ring was inactive up to 10 μM. The unsubstituted 4-methyl derivatives **B1** and **B5** were both inactive. Altogether, these data suggest that 1,2-dihydro-2-oxo-pyridine-3-carboxamides are versatile molecules that can selectively inhibit the endocannabinoid degrading enzymes FAAH, ABHD6 and ABHD12. Finally, we also investigated the effects of our compounds on the inhibition of AEA cellular uptake. Compounds **B1**, **B2** and **B4**

inhibited AEA uptake with a moderate potency. Nonetheless, due to their significant activity as FAAH inhibitors, a partial FAAH-dependent contribution in AEA uptake inhibition cannot be ruled out. Indeed, due to the tight interplay between FAAH inhibition and AEA uptake [34-36], it is impossible to undoubtedly differentiate between FAAH-dependent and FAAH-independent AEA uptake inhibition in our assay format. Therefore, we have not tested the most potent FAAH inhibitor **B3** for AEA uptake. However, compounds **B5** and **B6** showed sub-micromolar potencies in inhibiting AEA cell uptake without affecting FAAH up to 10 μM, thus representing potential selective AEA uptake inhibitors as compared to FAAH.

Altogether, our results show that the 1,2-dihydro-2-oxo-pyridine-3-carboxamide is a flexible scaffold that can be further exploited to design multi-target compounds in the ECS. Interestingly, the combinations of substituents that generate CBRs ligands also lead to the interaction with endocannabinoid degrading enzymes and/or AEA cell uptake. In agreement, compounds that were inactive at CBRs did not exhibit any effect on the other targets (Table 1,2). Our results thus suggest that the combination of a bulky substituent in position 4 with any substituent in position 5 have detrimental effects for the interactions with ECS proteins measured here. The presence of a methyl group in position 4 generated potent CB2R ligands poorly selective over CB1R, which also inhibited FAAH (Table 1 and Fig. 3). This type of polypharmacology was recently reported for a class of functionalized beta-caryophyllene derivatives [37]. Interestingly, the presence of a bromine atom or phenyl group in position 5 led to the moderate inhibition of ABHD12 which was selective over the other 2-AG hydrolytic enzymes ABHD6 and MAGL (Table 1 and Fig. 3). This combination of pharmacological effects *in vivo* could lead to an increase of AEA levels combined with a mild and cell-specific augmentation of 2-AG concentrations, which was shown to avoid CB1R tolerance in brain [36,38,39]. Other multi-target properties were shown by the 5-bromo-4-phenyl derivative **C3**, which behaved as moderately potent CB2R agonist and ABHD6 inhibitor (Table 1,2). Interestingly, compound **B5** and **B6** bearing the *p*-fluorobenzyl on the oxygen in

position 2 of the heterocyclic nucleus rather than on the N-1 of the 1,2-dihydro-2-oxo-pyridine ring exhibited two additional multi-target properties. Beyond the moderate interaction with CB1R and CB2R, **B5** inhibited AEA uptake with a sub-micromolar IC_{50} value without affecting FAAH up to 10 μM, similarly to compound **B6**. The latter showed also a selective inhibition of ABHD6 without affecting the other degrading enzymes up to 10 μM (Table 1, Fig. 3). The corresponding *N*-substituted compounds **B1** and **B2** inhibited AEA uptake and FAAH with similar potencies. Despite the small number of compounds tested, our data suggest that the shift of the *p*-fluorobenzyl group from nitrogen to the oxygen in position 2 of the heterocyclic ring generates relatively potent AEA uptake inhibitors which are at least 20-times more selective over FAAH.

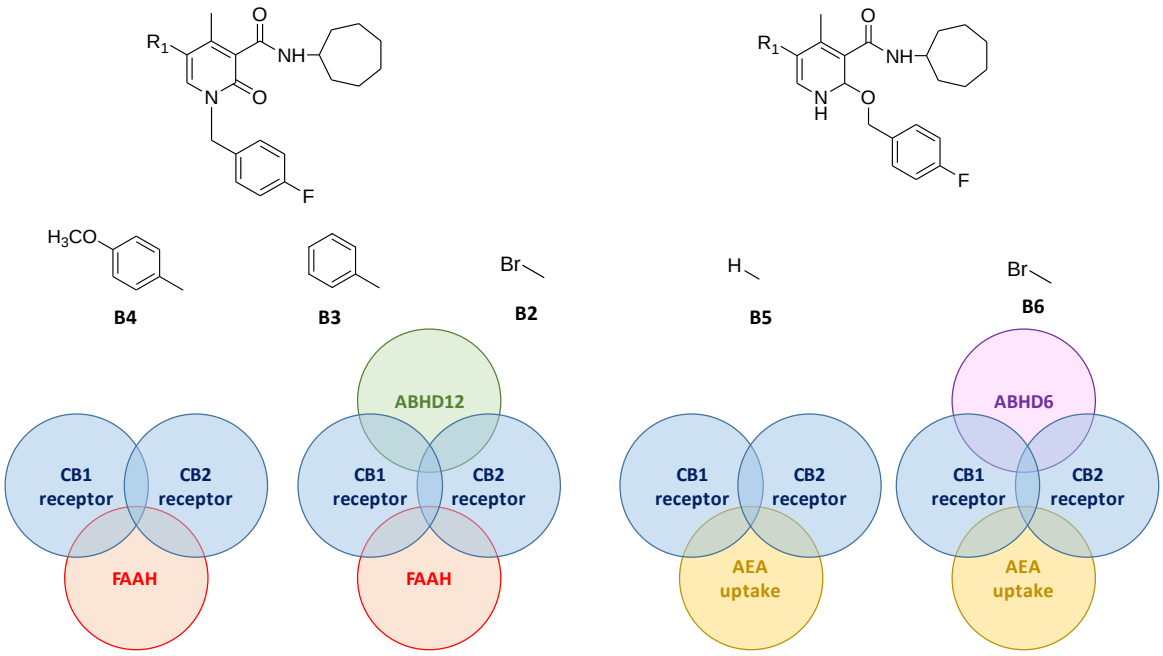

Figure 3. Summary of the most interesting polypharmacology properties observed with 1,2-dihydro-2-oxo-pyridine-3-carboxamides.

Overall, our study showed that the introduction of a small substituent as methyl in position 4 of the 1,2-dihydro-2-oxo-pyridine ring does not significantly affect the binding affinity and functional behavior at CB2R of 1,2-dihydro-2-oxo-pyridine-3-carboxamides as compared to the unsubstituted

analogs [25]. However, the new molecules exhibited unexpected and interestingly polypharmacology effects on endocannabinoid degrading enzymes and AEA cell uptake, suggesting interesting SAR properties of this scaffold which need to be further investigated (Fig. 3).

2.2.4. Cell viability assay

The 4-methyl derivatives **B1-B6**, that showed the best results in terms of binding properties on both CB1R and CB2R were tested to assess whether the observed activity on CBRs, would result into their different biological behavior. The selective CB2R inverse agonist 4-phenyl substituted compound **C1** and the CB2R neutral antagonist N-Cycloheptyl-5-(4-methoxyphenyl)-1-(4-fluorobenzyl)-pyridin-2(1H)-on-3-carboxamide (**MC21)** previously reported by us [25] were also assessed. First, we tested the compounds for their capability to inhibit viability of U251MG glioblastoma cell line, which mainly expresses CB1R [40], and that of U937 lymphoblastoid cells where, on the contrary, CB2R is predominantly expressed [41]. To this end, U251MG and U937 cells were incubated with the compounds. After 48 hours, the viable cell number was determined by MTT assay. Overall, the results showed that exposure to the compounds in a 0.6-40 μM concentration range led to a significant reduction in the number of viable U937 cells (Fig. 4, lower panel) but not of U251 cells for which a certain increase in cell proliferation was instead detected (Fig. 4, upper panel) in response to **B1**, **B2**, **B5** and **B6** treatment. As U937 cells exhibited CB2R but not CB1R, these results suggest that even though to a different extent, the cytotoxic activity of all tested compounds was mediated through the CB2R but not CB1R.

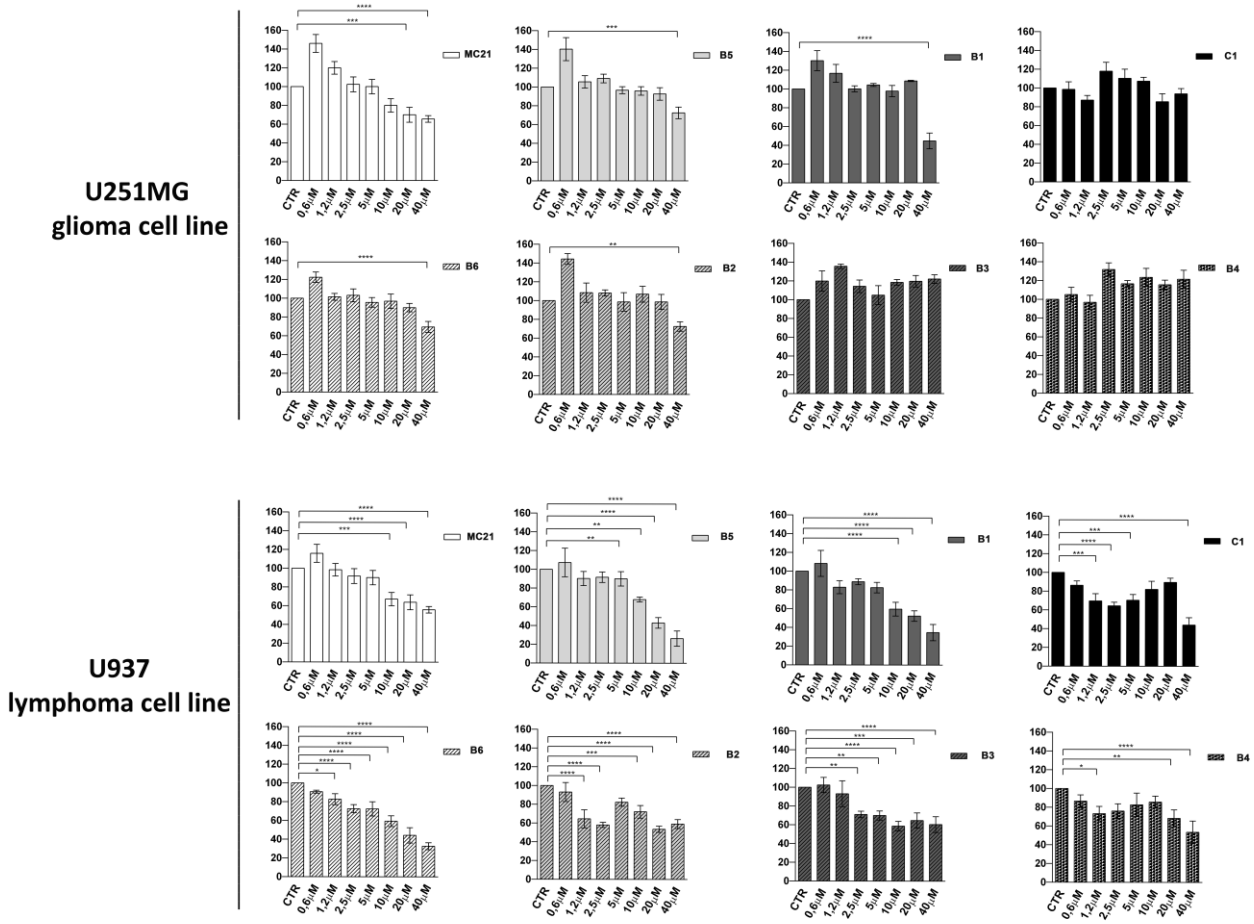

Figure 4. Effect of **MC21**, **B1-B6** and **C1** on cellular viability of human GBM (U251MG) and human lymphoblastoid U937 cells. U251MG cells (upper panel) and U937 cells (lower panel) were cultured for 48h in the presence of the indicated concentrations (0–40 μM) of the individual substances, before the assessment of MTT assay. Results are expressed as means ± SD of five independent experiments performed in triplicate and reported as percentage vs. the untreated control Then, the collected data were analyzed for statistical significance using ANOVA followed by Bonferroni correction for multiple comparisons. (ANOVA *P<0.05, **P<0.01 and ***P<0.001 vs. control).

We recently reported the new concept of CB1R behaving as a modulator both of cell proliferation and immune escape in glioma [42]. In particular, the use of the CB1R inverse agonist SR141761

suggested that CB1R blockage mediates both an anti-proliferative action and an immunomodulatory capacity, in terms of up-regulation of immunogenic signals on glioma cell surface [42]. Taking all these in account, we asked whether the residual CB1R activity of tested compounds might induce the expression of the NKG2D ligand MICA/B on the surface of U251MG glioma cells. Indeed, while the anti-proliferative action is related to CB1R-blocking, we cannot exclude that the immunogenic potential might be related at least in part to CB1R activation. So, by FACS analysis we monitored the cell surface expression of the NKG2D ligand MICA/B on untreated and compounds treated U251 glioma cells after 24 h of incubation to exclude that the possibility of observed effects were linked to the stress of dying cells. We specifically found that the incubation with CB1R agonists **B2**, **B4** and **B6**, resulted in a significant up-regulation of MICA/B expression on U251 cells in terms of Mean Fluorescence Intensity (MFI) (Fig. 5). These results could help clarifying some aspects of the effects shown by these new ECS modulators, which may be able to exert both cytostatic effects through CB2R and immunogenic activity mainly through CB1R modulation.

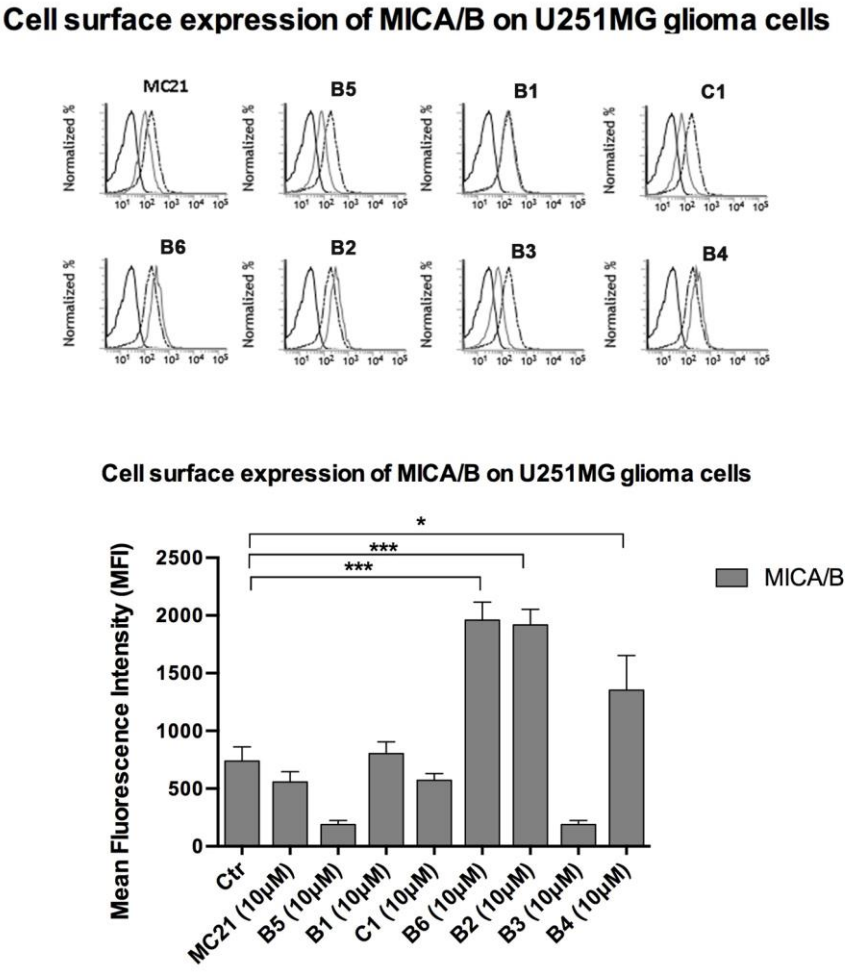

Figure 5. Effect of **MC21**, **B1-B6** and **C1** on cell surface expression of MICA/B on U251 glioma cells. Representative example for cytofluorimetric histogram profiles of MICA/B protein levels at the U251 cell surface of control (black long dash dot lanes) or cells treated with compound for 24 h (empty grey profiles) (upper panel). The mean fluorescence intensity (MFI) of U251 positive cells for MICA/B was calculated based on 3 independent experiments. Bar graphs report mean values ± SD (lower panel). Then, the collected data were analyzed for statistical significance using ANOVA followed by Bonferroni correction for multiple comparisons (ANOVA, (*$P < 0.05$, ***$P < 0.001$ compared with untreated cells).

2.3. In silico ADME profiling

In order to get a preliminary picture of the compounds' ADME profile, some of the most relevant physicochemical properties were predicted for the most active ligands. For instance, the software QikProp from Schrodinger suite [43] was used to calculate the octanol/water partition coefficient (expressed as logP), which is commonly used as an indicator of molecular lipophilicity, the aqueous solubility (expressed as logS) and the apparent permeability of the ligands through Caco-2 and MDCK (Madin-Darby canine kidney) cells, which are considered to be a good mimic of the gut-blood barrier and the blood-brain barrier, respectively [44]. Such properties are reported in Table 3, together with the Lipinski and Jorgensen rules violations.

As expected, all ligands showed high values of logP, and low values of logS, which are both in agreement with the substantial lipophilic character of the compounds that can be deduced by their chemical structure. Accordingly, very high permeability to both Caco-2 and MDCK cells was calculated for all ligands. Compound **B1** was unsurprisingly predicted to be the most soluble and the least lipophilic of the series, bearing only a methyl group and a hydrogen in position 4 and 5 of the oxopyridine core, respectively. Interestingly, compound **B5**, which is a structural isomer of **B1**, presented similar values of logP and logS but a higher permeability. The presence of a bromine atom in position 5 of the core determines an increased lipophilicity and a decreased solubility in **B2** and **B6**, with respect to their non-brominated analogues **B1** and **B5**. Interestingly, the presence of the bromine substituent seems to confer a particular boost to the MDCK apparent permeability of **B2** and **B6** and this is a highly desirable effect considering that the two ligands showed the best activity in inducing the expression of MICA/B on the surface of U251MG glioma cells. Compounds **B3** and **B4**, where the 4-methyl group was replaced by an aromatic substituent, showed the highest lipophilicity and the lowest solubility values. Overall, the physicochemical properties predicted for the compounds should be suitable for the activity of the ligands on the central nervous system. However, although all compounds have logP values in the range of 95% of known drugs, a lower

lipophilicity would be desirable for a good bioavailability and a low toxicity risk. In fact, all ligands but **B1** violated a Lipinski rule, having a logP value higher than 5. Moreover, derivatives with higher water solubility would be required in order perform *in vivo* studies on this series of compounds. Indeed, five ligands (**B2-B4**, **B6** and **C1**), violated a Jorgensen rule, presenting a logS value lower than -5.7, while **B3**, **B4** and **C1** showed solubility values that fall outside the range of 95% of known drugs (-6.5 < logS < 0.5). Based on these considerations, the series of compounds could be expanded introducing derivatives bearing more hydrophilic substituents, such as the morpholine ring of the recently reported CB2 ligand VL15 [45], with the aim of improving ADME profile and developing better candidates for in vivo studies.

Table 3. Predicted lipophilicity (logP), water solubility (logS), Caco-2 and MDCK cell apparent permeability, as well as rules violation of compounds **B1-B6** and **C1**.

Cmpd	logP	logS	Caco-2 (nm/s)	MDCK (nm/s)	RoF[a] violations	RoT[b] violations
B1	4.7	-5.6	2664.5	2573.3	0	0
B2	5.2	-6.4	2677.4	6182.6	1	1
B3	6.3	-7.5	2727.3	2638.9	1	1
B4	6.3	-7.6	2723.2	2634.5	1	1
B5	5.1	-5.4	4379.0	4281.1	1	0
B6	5.6	-6.1	4304.2	9848.6	1	1
C1	6.0	-6.7	3140.9	3073.9	1	1

[a]Lipinski rule of Five, [b] Jorgensen rule of Three.

2.4. Molecular Modeling Studies

To rationalize the structure-activity relationships (SARs) experimentally observed, a molecular docking analysis of the synthetized compounds was carried out into the three-dimensional structure of CB1R and CB2R.

Recently, the crystal structure of CB1R in complex with the antagonist AM6538 has been determined (PDB code: 5TGZ) [46]. To date, the CB2R subtype has not been crystallized yet. Thus, a homology model of this target has been developed by using CB1R structure as template, since the two receptors are endowed with a good sequence similarity (44% of amino acid sequence identity). Starting from the alignment shown in Figure S1 (Supporting information), an initial model of CB2R was created and subjected to a simulated annealing protocol by means of the software Modeller [47]. The model was inserted into a membrane bilayer and water environment and subjected to 100 ns of MD simulation with AMBER14 [48]. Before the simulation, geometry optimization of the CB2R model has been performed with a position constraint of 10 kcal/(mol·Å) applied to the protein α carbons, employing a total of 20'000 steps of energy minimization. The same analysis was applied to the CB1R-AM6538 complex in order to validate the procedure. The synthesized compounds were docked using AUTODOCK 4.2 into the CB1R and CB2R. For each ligand, a total of 200 different docking poses were generated and clustered with an RMSD threshold of 2.0 Å. For each compound, the top-scored pose was considered. Figure 6A shows the docking results obtained for compound **B2** into the CB1R and CB2R binding sites. Among all the compounds of this series, compound **B2** revealed the highest CB1R and CB2R affinity. In the CB1R model the compound is localized between the transmembrane domain (TM) 2, 3, 6 and 7 and shows a large number of lipophilic interactions. The *p*-fluorobenzyl substituent is directed towards the intracellular side of the receptor and interacts with V196 and L387 whereas the cycloheptyl group is inserted into a lipophilic cleft mainly delimited by T197, F268, W279, W356, L359 and M363. Finally, the 5-bromo-4-methyl-2-oxopyridine central core of the molecule shows additional lipophilic interactions with F102, M103, F268 and F379. The analysis of the docking results into the CB2R highlights that

this compound shows the same binding mode and the same interaction present in the CB1R (see Figure 6B). This result is in agreement with the analysis of the non-conserved residues around the compound. By applying a threshold of 4 Å around the hypothesized binding disposition of **B2**, there are only three non-conserved residues and their mutation does not affect the interactions of the compound, as the CB1R G166, L193 and S199 are changed in the CB2R with A83, I110 and T116, respectively (see Figure S1).

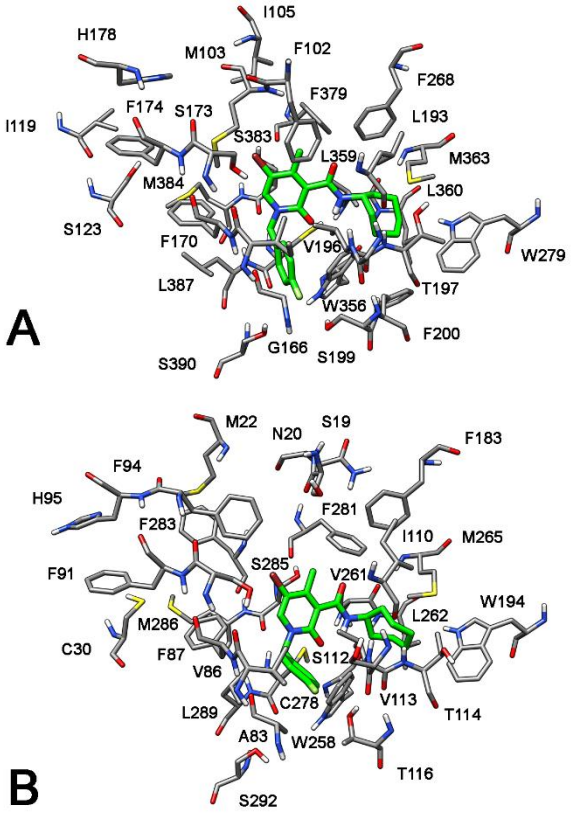

Figure 6. Top-scored poses of compound **B2** docked into CB2R (A) and CB1R (B).

As shown in Figure S2, the replacement of the 5-bromine atom with a bulkier group such as the phenyl ring as for compound **B3**, does not determine important modifications in the binding mode of the compound into both receptors as the phenyl ring fulfils the binding site cavity near the TM1, 2, 7 region (see Figure S2). The higher affinity for CB2R with respect to CB1R showed by this compound (3-fold selectivity) could be probably due to the interaction of the phenyl ring with the

F94 residue in the CB2R that is far away from the binding site in the CB1R. Differently, the substitution of the 4-methyl with a bulkier group such as the phenyl ring of compound **C3**, determines the total loss of affinity for both receptors. As shown in Figure S3, this substitution prevents, into both receptors, the maintenance of the binding disposition showed by the other two active compounds and this finding could be the reason of the low affinity of compound **C3**. Compounds **B1**-**B4** differ only for the R1 substitution and among them **B2** is the most active against CB1R. With respect to **B1**, the bromine atom of **B2** shows positive lipophilic interactions with the receptor, whereas its substitution with the phenyl and *p*-OCH_3phenyl fragment (compounds **B3** and **B4**) determines a slight decrease of activity probably due to the larger dimension of these substituents and the fact that they are directed towards the water exposed region of the binding site cavity. In CB2R, the presence of F94 near the TM1, 2, 7 region of the binding site limits the exposure to the solvent; this may explain why the different R1 substituents in **B1-B4** have a smaller impact in the affinity of the ligands for CB2R. Comparing the disposition of **C3** to that predicted for **B2** and **B3** it is possible to underline that the ligand leaves the lipophilic cleft in the TM3, 5, 6 region and moves towards the TM1, 2, 7 region.

Compound **B3** also shows a nanomolar inhibition activity against FAAH. The docking results for this compound suggest that the *p*-fluorobenzyl interacts with the catalytic S241 and shows lipophilic interactions with M191 (Figure 7). The cycloheptyl ring is directed towards the entrance of the binding site and does not show important interactions, whereas the 5-phenyl ring appears to have an important role as it is inserted in a lipophilic cleft delimited by F192, L380, F381 and F388. The replacement of the 4-methyl with a phenyl group determines the total loss of activity of the compound; as shown in Figure 7 the binding site region surrounding the 4-methyl group of **B3**, is very small and cannot allow the presence of a bulkier substituent. The docking analysis of **C5** clearly supports this hypothesis: as shown in Figure S4, this compound is not able to interact with the catalytic S241 and occupies a binding site cavity completely different from that occupied by **B3**.

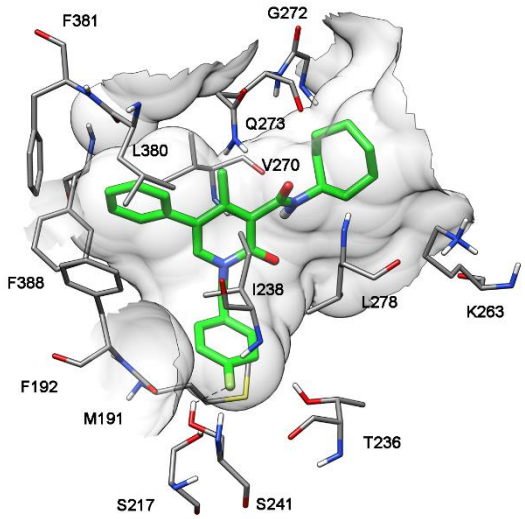

Figure 7. Top-scored pose of compound **B3** docked into FAAH.

3. Conclusion

The ECS represents one of the major neuromodulatory systems involved in different physiological and pathological processes and therefore it is a promising drug target. However, despite several attempts to pharmacologically modulate the main components of this system have been performed, the results obtained in pre-clinical and clinical settings were not completely satisfying in terms of safety or efficacy. Alternative pharmacological approaches have been explored with the aim of modulating two or more components of the ECS [49-51]. The present study describes a series of new 4-substituted and 4,5-disubstituted-1,2-dihydro-2-oxo-pyridine-3-carboxamide derivatives that showed a broad spectrum of affinity and functional activity towards both CBRs and interesting effects on the other components of the ECS. In particular, the combination of a methyl group in position 4, a bulky substituent in position 5 and the *p*-fluorobenzyl group in the N-1 position of the 1,2-dihydro-2-oxo-pyridine ring (**B3** and **B4** derivatives) determine a high affinity for both CBRs and high potency to inhibit the main AEA

hydrolytic enzyme, fatty acid amide hydrolase (FAAH). Furthermore, in one case (**B4** derivative), these activities were associated to moderate low micromolar inhibition of the minor 2-AG hydrolytic enzymes and ABHD12. Interestingly, the compounds that bear the *p*-fluorobenzyl on the oxygen in position 2 of the heterocyclic nucleus (**B5** and **B6**), beyond the moderate interaction with both CBRs, showed to inhibit AEA uptake with a sub-micromolar IC_{50} value without affecting FAAH activity up to 10 μM and one of them (**B6** derivative) displayed also a selective inhibition of ABHD6.

Moreover, the 4-methyl derivatives **B1**, **B2**, **B5** and **B6** that showed the best results in terms of binding properties and agonist/partial agonist behavior on both CBRs displayed a significant reduction of U937 cell viability where CB2R is predominantly expressed, but not of U251 cells, which mainly express CB1R. Furthermore, the CB1R full agonists **B2**, **B4** and **B6** showed a significant up-regulation of MICA/B expression on U251 cells. These results indicated the polyhedral effects of these compounds, which can exert both cytostatic effects through CB2R and immunogenic activity mainly through CB1R modulation.

Altogether, this new series of 4-substituted and 4,5-disubstituted-1,2-dihydro-2-oxo-pyridine-3-carboxamide derivatives present diverse and intriguing multi-target profiles in the ECS, despite the limited number of compounds that have been assessed. This scaffold may represent a useful starting point to generate more derivatives in order to further explore the different multi-target approaches and assess their potential pharmacological advantages and disadvantages as compared to the single target approach. Moreover, novel chemical probes that differentially target this complex network of lipid pathways may be useful to better understand endocannabinoid function.

4. Experimental

4.1. Chemistry

Commercially available reagents were purchased from Sigma Aldrich or Alfa Aesar and used without purification. ^{1}H NMR and ^{13}C NMR were recorded at 400 and 100 MHz respectively, on a Bruker AVANCE III™ 400 spectrometer. Chemical shift (δ) are reported in parts per million related to the residual solvent signal, while coupling constants (J) are expressed in Hertz (Hz). Microwave-assisted reactions were run in a Biotage® microwave synthesizer. All final compounds were analyzed by HPLC, showing a purity ≥ 95%. A Bechman HPLC instrument equipped with a System Gold Solvent Delivery module (Pumps) 125, System Gold UV/VIS Detector 166, Detector set to 278 nm, was employed. Analyses were performed on a reverse phase C18 column (Phenomenex 250 x 4.6 mm, 5 mm particle size, Gemini). The mobile phase was constituted by a mixture of H_2O/AcOH (0.1% v/v) (eluent A) and ACN (eluent B). A gradient starting from 50% of B, changing to 100% of B over 20 min., and returning to the initial conditions over 10 min., was used for compounds The flow rate was 1.0 ml/min. Organic solutions were dried over anhydrous Na_2SO_4. Evaporation was carried out in vacuo using a rotating evaporator. Silica gel flash chromatography was performed using silica gel 60 Å (0.040-0.063 mm; MERK). Reactions was monitored by TLC on Merck aluminium silica gel (60 F254) plates that were visualized under a UV lamp (λ = 254 nm). Melting points were determined on a Kofler hot-stage apparatus and are uncorrected.

*4.1.1. 2-Hydroxy-3-cyano-4-methylpyridine (**1**)*

A mixture of 4,4-dimethoxyl-2-butanone (2.0 g, 15.13 mmol), cyanoacetamide (1.6 g, 18.92 mmol), ammonium acetate (79.3 mg, 1.03 mmol), acetic acid (0.6 mL) in anhydrous toluene (12.4 mL) was refluxed under stirring for 8 h, removing the produced water by Dean-Stark apparatus. When this step was finished, the reaction mixture was evaporated under reduced pressure, the

residual oil was cooled to room temperature and EtOH (7.0 mL) was added under stirring at 25 °C. After that, H_2SO_4 50% (2.6 mL) was added slowly and the mixture was heated at 50 °C under stirring for 3 h. The reaction mixture was then cooled to 5 °C, and water (1.3 mL) was added slowly. The obtained brown solid was purified by crystallization in EtOH to obtain 2-hydroxy-3-cyano-4-methylpyridine **1** (0.900 g, yield: 45%); mp: 233-236 °C. ^{1}H-NMR (400 MHz, DMSO): δ 12.58 (bs, 1H, NH), 8.04 (d, *J* = 7.4 Hz, 1H, H6 Py), 6.24 (d, *J* = 7.4 Hz, 1H, H5 Py), 2.31 (s, 3H, CH_3).

*4.1.2. 4-Methyl-1,2-dihydro-2-oxo-pyridine-3-carboxylic acid (**2**)*

4-methylpyridine **1** (1.0 g, 7.46 mmol) was heated in H_2SO_4 50% (1.4 mL) at 120 °C for 8 h. After that, the reaction mixture was cooled at room temperature and few drops of water were added at 0 °C. The formed precipitate was filtered *under vacuum*, washed with water and dried to afford compound **2** (0.740 g, yield: 65%) as white solid which was used without purification. ^{1}H-NMR (400 MHz, DMSO): δ 13.33 (bs, 1H, COOH), 11.88 (bs, 1H, NH), 8.30 (d, *J* = 7.6 Hz, 1H, H6 Py), 6.57 (d, *J* = 7.6 Hz, 1H, H5 Py), 2.41 (s, 3H, CH_3).

*4.1.3 Methyl 4-methyl-1,2-dihydro-2-oxo-pyridine-3-carboxylate (**3**)*

A solution of 4-methyl-1,2-dihydro-2-oxo-pyridine-3-carboxylic acid **2** (0.120 g, 0.78 mmol) in MeOH (0.5 mL) and concentrated H_2SO_4 (0.2 mL) was refluxed at 85 °C for 12 h or heated in a microwave reactor at 100° C for 50 minutes (power = 200 W, pressure = 100 psi). After cooling to room temperature, the mixture was treated with solid Na_2CO_3 until pH = 7-8 and extracted with CH_2Cl_2. The organic layer was dried over anhydrous Na_2SO_4, filtered and evaporated under reduced pressure to give **3** (83.3 mg, yield: 80%) as a white solid. ^{1}H-NMR: ($CDCl_3$) δ 8.20 (d, *J* = 7.6 Hz, 1H, H6 Py), 6.28 (d, *J* = 7.6 Hz, 1H, H5 Py), 3.90 (s, 3H, $COOCH_3$), 2.48 (s, 3H, CH_3).

*4.1.4. N-Cycloheptyl-1,2-dihydro-4-Methyl-2-oxo-pyridine-3-carboxamide (**4**)*

The 1,2-dihydro-2-oxo-pyridine **3** (0.187 g, 1.13 mmol) was suspended in cyclohepthylamine (0.5 mL, 3.67 mmol) and heated at 150° C for 48 h or in a microwave reactor at 130° C for 30 minutes (power = 140 W, pressure = 100 psi). After cooling to room temperature, the reaction mixture was kept in an ice-water bath and treated with 10% HCl until pH = 1-2. The precipitated solid was collected by filtration, washed with water and dried *under vacuum* to afford the pure amide **4** (80.0 mg, yield: 31%) as a white solid. ^{1}H-NMR (400 MHz, $CDCl_3$): δ 12.96 (bs, 1H, NH Py), 9.63 (bd, 1H, CONH), 8.55 (d, *J* = 7.6 Hz, 1H, H6 Py), 6.36 (d, *J* = 7.6 Hz, 1H, H5 Py), 4.25-4.23 (m, 1H, NCH), 2,45 (s, 3H, CH_3), 1.51-1.98 (m, 12H, cycloheptyl).

*4.1.5. General procedure for the synthesis of N_1-substituted **B1, B2** and O-substituted **B5, B6** pyridine-3-carboxamide derivatives*

Cesium fluoride (0.30 mmol) was added to a solution of the 3-carboxamide derivative **4** or **5** (0.3 mmol) in anhydrous DMF (0.9 mL). After 1 h, *p*-fluorobenzyl chloride (0.90 mmol) was added, and the resulting mixture was left under stirring at 25 °C for 12 h. After cooling to room temperature, the reaction mixture was concentrated under reduced pressure, treated with water, and then extracted with dichloromethane. The organic layer was dried over anhydrous Na_2SO_4, filtered, and evaporated under reduced pressure to give a residue which was purified by flash chromatography.

*4.1.5.1. N-cycloheptyl-1,2-dihydro-1-(4-fluorobenzyl)-4-methyl-2-oxo-pyridine-3-carboxamide (**B1**) and N-cycloheptyl-2-(4-fluorobenzyloxy)-4-methyl-pyridine-3-carboxamide (**B5**)*

Purified by flash column chromatography on silica gel (petroleum ether/ethyl acetate from 8:2 to 5:5). **B1**: yield 53%. ^{1}H NMR (400 MHz, $CDCl_3$): δ 9.72 (bd, 1H, CONH), 8.45 (d, *J* = 7.6 Hz, 1H, H6 Py), 7.11-6.99 (m, 4H, Ar), 6.30 (d, *J* = 7.6 Hz, 1H, H5 Py), 5.35 (s, 2H, N-CH_2), 4.14-4.11 (m,

1H, N-CH), 2.35 (s, 3H, CH_3), 1.48-2.03 (m, 12H, cycloheptyl). ^{13}C-NMR (100 MHz, $CDCl_3$): δ 162.50 (d, *J* = 245.0 Hz), 163.44, 163.07, 150.59, 143.35, 131.46 (d, *J* = 3.2 Hz), 128.29 (d, *J* = 8.4 Hz), 119.36, 116.28 (d, *J* = 22.1 Hz), 108.38, 50.72, 47.40, 35.27, 28.44, 24.56, 21.42. HPLC analysis: retention time =11.94 min; peak area, 98.7% (280 nm). **B5**: yield: 30%. ^{1}H NMR ($CDCl_3$) δ 8.39 (d, *J* = 8.0 Hz, 1H, H6 Py), 7.90 (bd, 1H, CONH), 7.48-7.42 (m, 2H, Ar), 7.13-7.07 (m, 2H, Ar), 6.90 (d, *J* = 8.0 Hz, 1H, H5 Py), 5.43 (s, 2H, O-CH_2), 4.17-4.08 (m, 1H, N-CH), 2.50 (s, 3H, CH_3), 1.85-1.34 (m, 12H, cycloheptyl). ^{13}C NMR (100 MHz, $CDCl_3$): δ 163.00 (d, *J* = 246.0 Hz), 162.79, 159.49, 159.44, 142.06, 132.48, 130.85 (d, *J* = 8.4 Hz), 117.49, 115.77 (d, *J* = 22.1 Hz), 113.53, 68.19, 50.07, 34.85, 28.39, 24.24, 23.85. HPLC analysis: retention time = 12.10 min; peak area, 99.15% (280 nm).

*4.1.5.2. 5-Bromo-N-cycloheptyl-1,2-dihydro-1-(4-fluorobenzyl)-4-methyl-2-oxo-pyridine-3-carboxamide (**B2**) and 5-bromo-N-cycloheptyl-2-(4-fluorobenzyloxy)-4-methyl-pyridine-3-carboxamide (**B6**)*

Purified by flash column chromatography on silica gel (petroleum ether/ethyl acetate 9:1). **B2**: yield 32%. ^{1}H NMR (400 MHz, $CDCl_3$): δ 9.61 (bd, 1H, CONH), 8.66 (s, 1H, H6 Py), 7.03 -7.13 (m, 4H, Ar), 5.43 (s, 2H, N-CH_2), 4.11-4.17 (m, 1H, N-CH), 2.53 (s, 3H, CH_3), 1.51-2.05 (m, 12H, cycloheptyl). ^{13}C NMR (100 MHz, $CDCl_3$): δ 162.45 (d, *J* = 245.0 Hz), 162.17, 161.52, 148.43, 146.63, 130.82 (d, *J* = 2.8 Hz), 128.13 (d, *J* = 8.4 Hz), 120.21, 116.26 (d, *J* = 22.1 Hz), 101.97, 50.70, 48.81, 35.01, 28.25, 24.32, 20.93. HPLC analysis: retention time = 11.53 min; peak area, 98.5% (280 nm). **B6**: yield 41%. ^{1}H NMR (400 MHz, $CDCl_3$): δ 8.57 (s, 1H, H6 Py), 7.81 (bd, 1H, CONH), 7.49-7.43 (m, 2H, Ar), 7.14-7.08 (m, 2H, Ar), 5.42 (s, 2H, O-CH_2), 4.17-4.09 (m, 1H, N-CH), 2.61 (s, 3H, CH_3), 1.86-1.37 (m, 12H, cycloheptyl). ^{13}C NMR (100 MHz, $CDCl_3$): δ 163.03 (d, *J* = 246.0 Hz), 161.36, 158.01, 157.60, 144.82, 131.97 (d, *J* = 3.2 Hz), 130.85 (d, *J* = 9.0 Hz),

115.81 (d, *J* = 21.9 Hz), 115.53, 113.55, 68.67, 50.16, 34.72, 28.32, 24.57, 23.75. HPLC analysis: retention time = 11.89 min; peak area, 99.0% (280 nm).

*4.1.6. General procedure for the preparation of 5-bromo-3-carboxamide derivatives **5**, **C3** and **C4**.*

To a solution of the suitable 1,2-dihydro-2-oxo-pyridine-3-carboxamide (**4**, **C1** or **C2**) (1.78 mmol) in $CHCl_3$ (3.0 mL) was added dropwise a solution of bromine (0.1 mL, 1.78 mmol) in $CHCl_3$ (1.8 mL) and the mixture was left under stirring at room temperature for 12 h. The reaction mixture was then treated with an aqueous solution of sodium bisulfate and extracted with $CHCl_3$. The organic layer was washed with water, dried over anhydrous Na_2SO_4 and evaporated under reduced pressure. The obtained residue was triturated with high boiling point petroleum ether to afford the pure desired compound.

*4.1.6.1. 5-Bromo-N-cycloheptyl-1,2-dihydro-4-methyl-2-oxo-pyridine-3-carboxamide (**5**)*

Yield 99 %. ^{1}H NMR (400 MHz, $CDCl_3$,): δ 13.40 (bs, 1H, NH Py), 9.45 (bd, 1H, CONH), 8.65 (s, 1H, H6 Py), 4.21-4.18 (m, 1H, NCH), 2.53 (s, 3H, CH_3), 1.88-1.57 (m, 12H, cycloheptyl).

*4.1.6.2. 5-Bromo-N-cycloheptyl-1,2-dihydro-1-(4-fluorobenzyl)-2-oxo-4-phenyl-pyridine-3-carboxamide (**C3**)*

Yield 63%. ^{1}H NMR (400 MHz, $CDCl_3$) δ 7.60 (s, 1H, H6 Py), 7.43-7.37 (m, 5H, Ar), 7.24-7.19 (m, 2H), 7.12-7.06 (m, 2H), 6.75 (bd, 1H, CONH), 5.13 (s, 2H, NCH_2), 3.90-3.87 (m, 1H, NCH), 1.36-1.74 (m, 12H, cycloheptyl). ^{13}C NMR (100 MHz, $CDCl_3$): δ 162.99 (d, *J* = 245.0 Hz), 162.75, 159.80, 152.98, 137.65, 137.44, 131.07 (d, *J* = 3.2 Hz), 130.73 (d, *J* = 8.4 Hz), 128.74, 128.17, 127.88, 127.41, 116.27 (d, *J* = 21.0 Hz), 102.06, 52.10, 50.49, 34.75, 28.15, 24.05. HPLC analysis: retention time = 11.46 min; peak area, 97.8% (280 nm).

*4.1.6.3. 5-Bromo-N-cycloheptyl-1,2-dihydro-1-(4-fluorobenzyl)-4-(4-methoxyphenyl)-2-oxo-pyridine-3-carboxamide (**C4**)*

Yield 95%. ^{1}H NMR: (400 MHz, $CDCl_3$) δ 7.59 (s, 1H, H6 Py), 7.40-7.36 (m, 2H, Ar), 7.18-7.15 (m, 2H, Ar), 7.10-7.06 (m, 2H, Ar), 6.93-6.91 (m, 2H, Ar), 6.55 (bd, 1H, CONH), 5.11 (s, 2H, N-CH_2), 3.95-3.92 (m, 1H, NCH), 3.81 (s, 3H, OCH_3), 1.80-1.21 (m, 12H, cycloheptyl). ^{13}C NMR (100 MHz, $CDCl_3$): δ 163.23, 160.03, 159.70, 152.59, 137.60, 131.12, 130.72 (d, *J* = 8.4 Hz), 129.51, 129.42, 128.50, 127.63, 116.25 (d, *J* = 22.1 Hz), 113.66, 102.57, 55.36, 52.03, 50.60, 34.77, 28.19, 24.06. HPLC analysis: retention time = 11.86 min; peak area, 98.5% (280 nm).

*4.1.7. General procedure for the synthesis of 5-substituted 3-carboxamide derivatives **B3, B4, C5** and **C6***

A mixture of PPh_3 (67.8 mg, 0.26 mmol) and $Pd(OAc)_2$ (11.7 mg, 0.049 mmol) in 1.7 mL of anhydrous toluene was stirred at room temperature under nitrogen flux. After 15 minutes, the 5-bromo derivative **B2** for **B3** and **B4**, or **C3** for **C5** and **C6** (75.0 mg, 0.17 mmol), anhydrous K_2CO_3 (0.26 mmol) and suitable arylboronic acid (0.34 mmol) were added to the mixture. The reaction was heated at 100 °C under stirring for 12 h. After cooling to room temperature, the reaction mixture was treated with water and extracted with CH_2Cl_2. The combined organic layers were washed with brine, dried over anhydrous Na_2SO_4, and evaporated under reduced pressure. The residue was purified by flash chromatography.

*4.1.7.1. N-Cycloheptyl-1,2-dihydro-1-(4-fluorobenzyl)-4-methyl-2-oxo-5-phenyl-pyridine-3-carboxamide (**B3**)*

Purified by flash chromatography on silica gel (petroleum ether/ ethyl acetate 7:3). Yield 96%. ^{1}H NMR (400 MHz, $CDCl_3$): δ 9.82 (bd, 1H, CONH), 8.51 (s, 1H, H6 Py), 7.42-7.32 (m, 3H, Ar),

7.23-7.20 (m, 2H, Ar), 7.16-7.12 (m, 2H, Ar), 7.07-7.04 (m, 2H, Ar), 5.46 (s, 2H, N-CH_2), 4.14-4.11 (m, 1H, N-CH), 2.30 (s, 3H, CH_3), 2.02-1.52 (m, 12H, cycloheptyl). ^{13}C NMR (100 MHz, $CDCl_3$): δ 162.31 (d, *J* = 245.0 Hz), 162.73, 162.60, 147.45, 145.20, 138.15, 131.37 (d, *J* = 4.0 Hz), 129.73, 128.76, 128.08 (d, *J* = 8.4 Hz), 127.82, 122.07, 118.65, 116.12 (d, *J* = 21.8 Hz), 50.54, 47.88, 35.08, 28.26, 24.33, 18.69.HPLC analysis: retention time = 12.01 min; peak area, 98.7% (280 nm).

*4.1.7.2. N-Cycloheptyl-1,2-dihydro-1-(4-fluorobenzyl)-5-(4-methoxyphenyl)-4-methyl-2-oxo-pyridine-3-carboxamide (**B4**)*

Purified by column chromatography on silica gel (petroleum ether/ethyl acetate 8:2). Yield 54%. ^{1}H-NMR (400 MHz, $CDCl_3$,): δ 9.80 (bd, 1H, CONH), 8.50 (s, 1H, H6 Py). 7.36-6.91 (m, 8H, Ar), 5.48 (s, 2H, N-CH_2), 4.18-4.14 (m, 1H, N-CH), 3.84 (s, 3H, OCH_3), 2.30 (s, 3H, CH_3) 2.05-1.43 (m, 12H, cycloheptyl). ^{13}C NMR (100 MHz, $CDCl_3$): δ 162.73, 159.23, 147.08, 145.60, 141.30, 131.20, 130.88, 130.00, 129.50, 128.04 (d, *J* = 8.4 Hz), 116.36 (d, *J* = 22.1 Hz), 114.73, 116.15, 114.16, 55.47, 50.90, 35.10, 28.29, 24.35, 23.00, 18.73. HPLC analysis: retention time = 11.89 min; peak area, 97.9% (280 nm).

*4.1.7.3. N-Cycloheptyl-1,2-dihydro-4,5-diphenyl-1-(4-fluorobenzyl)-2-oxo-pyridine-3-carboxamide (**C5**)*

Purified by column chromatography on silica gel (ethyl acetate/petroleum ether 7:3). Yield 91%. ^{1}H NMR (400 MHz, $CDCl_3$): δ 7.44-7.40 (m, 2H, Ar), 7.34 (s, 1H, H6 Py), 7.21-7.04 (m, 10H, Ar), 6.85-6.82 (m, 2H, Ar), 6.39 (bd, 1H, CONH), 5.19 (s, 2H, N-CH_2), 3.94-3.88 (m, 1H, NH-CH), 1.74-1.17 (m, 12H, cycloheptyl). ^{13}C NMR (100 MHz, $CDCl_3$): δ 164.29, 162.81 (d, *J* = 246.0 Hz), 160.09, 151.82, 136.69, 136.63, 136.28, 131.90, 131.72 (d, *J* = 3.2 Hz), 130.66 (d, *J* = 8.4 Hz),

129.71, 128.70, 128.13, 127.91, 127.15, 126.85, 122.25, 116.06 (d, *J* = 21.0 Hz), 52.00, 50.40, 34.76, 28.18, 24.03. HPLC analysis: retention time = 11.88 min; peak area, 97.8% (280 nm).

*4.1.7.4. N-Cycloheptyl-1,2-dihydro-1-(4-fluorobenzyl)-5-(4-methoxyphenyl)-2-oxo-4-phenyl-pyridine-3-carboxamide (**C6**)*

Purified by by column chromatography on silica gel (ethyl acetate/petroleum ether 6:4). Yield 70%. ^{1}H NMR (400 MHz, $CDCl_3$): δ 7.46-7.41 (m, 2H, Ar), 7.31 (s, 1H, H6 Py), 7.23-7.19 (m, 3H, Ar), 7.11-7-06 (m, 4H, Ar), 6.78-6.75 (m, 2H, Ar), 6.71-6.66 (m, 2H, Ar), 6.43 (bd, 1H, CONH), 5.18 (s, 2H, N-CH_2), 3.92-3.89 (m, 1H, N-CH), 3.75 (s, 3H, OCH_3), 1.72-1.12 (m, 12H, cycloheptyl). ^{13}C NMR (100 MHz, $CDCl_3$): δ 162.82, 162.37, 162.30 (d, *J* = 244.0 Hz), 158.64, 150.22, 145.97, 133.58, 132.64 (d, *J* = 4.1 Hz), 130.93, 130.01, 129.95, 129.54, 128.78 (d, *J* = 8.4 Hz), 128.60, 122.11, 120.65, 115.66 (d, *J* = 22.1 Hz), 113.69, 55.40, 50.81, 49.40, 35.28, 28.44, 24.55. HPLC analysis: retention time = 11.85 min; peak area, 98.4% (280 nm).

*4.1.8. 1,2-dihydro-1-(4-fluorobenzyl)-2-oxo-pyridine-3-carboxylic acid (**12**)*

Commercial available 2-hydroxynicotinic acid (1.5 g, 10.78 mmol) was dissolved in anhydrous DMF (20.0 mL) and then NaH (650.0 mg, 27.08 mmol) was slowly added. After 1 h at room temperature, *p*-fluorobenzyl chloride (1.5 mL, 12.52 mmol) was added and the reaction mixture was heated under stirring at 50 °C for 12 h. After cooling to room temperature, the reaction mixture was evaporated under reduced pressure affording a white solid that was treated with a solution of 10% NaOH (20.0 mL) and heated at reflux for 4 h. Then the mixture was cooled at room temperature and acidified with concentrated HCl until pH = 1-2. The obtained solid was filtered *under vacuum*, washed with water and dried to afford pure compound **12** (2.6 g, yield: 96%). ^{1}H NMR (400 MHz, DMSO): δ 12.02 (bs, 1H, COOH), 8.42-8.47 (m, 2H, , H4 and H6 Py) 7.22-7.50 (m, 4H, ArH), 6.83-6.80 (m, 1H, H5 Py), 5.34 (s, 2H, N-CH_2).

*4.1.9. N-Cycloheptyl-1,2-dihydro-1-(4-fluorobenzyl)-2-oxo-pyridine-3-carboxamide (**13**)*

To a solution of the 1,2-dihydropyridine-3-carboxylic acid **12** (3.40 g, 13.76 mmol) in anhydrous DMF (40.0 mL) were added DIPEA (7.2 mL, 41.28 mmol) and TBTU (4.40 g, 13.76 mmol) at 0 °C and under nitrogen flux. The reaction mixture was stirred at 0 °C for 30 minutes. Then cycloheptylamine (1.8 mL, 13.76 mmol) was added at 0 °C, and the reaction mixture was stirred at room temperature for 12 h. After evaporation of the solvent under reduced pressure, the crude residue was purified by flash column chromatography on silica gel using ethyl acetate/petroleum ether (6:4) as eluent, to obtain the amide **12** (3.30 g, yield 71%) as a brown oil. ^{1}H NMR (400 MHz, $CDCl_3$,): δ 9.73 (bd, 1H, CONH), 8.53 (m, 1H, H4 Py), 7.48-7.44 (m, Hz, 1H, H6 Py), 7.03-7.29 (m, 4H, Ar), 6.42-6.39 (m, 1H, H5 Py), 5.18 (s, 2H, CH_2), 4.15-4.12 (m, 1H, NCH), 1.53-2.02 (m, 12H, cycloheptyl).

*4.1.10. General procedure for the synthesis of 4-aryl-1,2-dihydro-2-oxo-pyridine-3-carboxamides **C1** and **C2***

To a solution of *N*-Cycloheptyl-carboxamide **13** (3.86 mmol) in anhydrous THF (28.2 mL), copper(I) iodide (0.75 mmol) and lithium bromide (0.75 mmol) were added under nitrogen atmosphere. The solution was cooled to -40 °C and the suitable arylmagnesium bromide (6.18 mmol) was added dropwise. The reaction mixture was stirred at -40 °C for 6 h, warmed up to room temperature and then a 20% solution of ammonium chloride (19.0 mL) and diethyl ether (24 mL) were added. The organic phase was separated and the water layer was extracted two times with diethyl ether (2 x 24 mL). The organic layers were collected and washed with 20% solution of ammonium chloride (45 mL), water (45 mL), with a 10% solution of hydrochloric acid (2 x 45 mL),

water (45 mL) and finally with brine. Afterwards the organic layer was dried over anhydrous Na_2SO_4, evaporated *under vacuum* and purified by flash chromatography.

*4.1.10.1.. N-Cycloheptyl-1,2-dihydro-1-(4-fluorobenzyl)-2-oxo-4-phenyl-pyridine-3-carboxamide (**C1**).*

Purified by column chromatography on silica gel (toluene/ethyl acetate 3:7). Yield 92%. ^{1}H NMR (400 MHz, $CDCl_3$): δ 7.46 (bd, 1H, CONH), 7.40-7.33 (m, 8H, Ar, H5 Py), 7.09-7.03 (m, 2H, Ar) 6.23 (d, 1H, *J* = 7.2 Hz, H4 Py), 5.15 (s, 2H, N-CH_2), 3.99-3.96 (m, 1H, N-CH), 1.89-1.25 (m, 12H, cycloheptyl). ^{13}C NMR (100 MHz, $CDCl_3$): δ 163.94, 163.81, 161.50, 154.32, 139.41, 136.87, 131.71, 130.40 (d, *J* = 9.0 Hz), 128.70, 128.40, 127.40, 123.85, 116.13 (d, *J* = 22.1 Hz), 109.93, 51.97, 50.52, 34.93, 28.18, 24.18. HPLC analysis: retention time = 12.03 min; peak area, 98.6% (280 nm).

*4.1.10.2. N-Cycloheptyl-1,2-dihydro-1-(4-fluorobenzyl)-4-(4-methoxyphenyl)-2-oxo-pyridine-3-carboxamide (**C2**).*

Purified by column chromatography on silica gel (ethyl acetate/petroleum ether 7:3). Yield 13%. ^{1}H NMR: (400 MHz, $CDCl_3$,): δ 7.35-7.28 (m, 6H, CONH, H6 Py and Ar), 7.08-7.03 (m, 2H, Ar), 6.91-6.88 (m, 2H, Ar), 6.23 (d, *J* = 6.8 Hz, 1H, H5 Py), 5.14 (s, 2H, N-CH_2), 4.02-3.98 (m, 1H, N-CH), 3.82 (s, 3H, OCH_3), 1.93-1.40 (m, 12H, cycloheptyl). ^{13}C NMR (100 MHz, $CDCl_3$): δ 164.27, 161.35, 160.19, 162.71 (d, *J* = 246.0 Hz), 153.41, 136.74, 131.76 (d, *J* = 4.0 Hz), 131.22, 130.26 (d, *J* = 9.1 Hz), 129.02, 123.55, 116.01 (d, *J* = 21.0 Hz), 113.88, 109.75, 55.36, 51.77, 50.56, 34.89, 28.13, 24.14. HPLC analysis: retention time = 11.89 min; peak area, 98.4% (280 nm).

4.2. CB1R and CB2R binding assays.

Receptor binding experiments were performed with membrane preparations as previously reported [37]. Briefly, clean membranes expressing *h*CB_1 or *h*CB_2 were re-suspended in binding buffer (50 mM Tris-HCl, 2.5 mM EDTA, 5 mM $MgCl_2$, 0.5%[1] fatty acid-free bovine serum albumin (BSA), pH 7.4) and incubated with vehicle or compounds and 0.5 nM of [^{3}H]CP55,940 for 90 min at 30 °C. Non-specific binding was determined in the presence of 10 μM of WIN55,512. After incubation, membranes were filtered through a pre-soaked 96-well microplate bonded with GF/B filters under vacuum and washed twelve times with 150 μL of ice-cold binding buffer. The radioactivity was measured and the results expressed as [^{3}H]CP55,940 binding.

4.3. Functional activity at CB1R and CB2R

Assays were performed as previously described [52]. Briefly, *h*CB_1- and *h*CB_2-expressing membranes (5 μg) were diluted in binding buffer (50 mM Tris-HCl, 3 mM $MgCl_2$, 0.2 mM EDTA, and 100 mM NaCl at pH 7.4 plus 0.5% fatty acid-free BSA) in the presence of 10 μM of GDP and 0.1 nM of [^{35}S]GTPγS. The mixture was kept on ice until the binding reaction was started by adding the vehicle or compounds. Non-specific binding was measured in the presence of 10 μM of GTPγS. The tubes were incubated at 30 °C for 90 min. The reaction was stopped by rapid filtration through a 96-well microplate bonded with GF/B filters previously pre-soaked with washing buffer (50 mM of Tris-HCl pH 7.4 plus 0.1% fatty acid-free BSA). The filters were washed six times with 180 μL of washing buffer under vacuum. The radioactivity was measured, and the results were expressed as [^{35}S]GTPγS binding.

4.4. Enzymatic assays.

FAAH, MAGL and ABHDs activity assays were performed as previously described [36]. Briefly, FAAH and MAGL activity assays were performed using U937 cell homogenate (100 μg) which were diluted in 200 μL of Tris–HCl 10 mM, EDTA 1 mM, pH 8 containing 0.1% fatty acid-free BSA. Compounds were added at the screening concentration of 10 μM and incubated for 30 min at 37 °C. Then, 100 nM of AEA containing 1 nM of [ethanolamine-1-^{3}H]AEA as a tracer for FAAH or 1 μM of 2-OG containing 1 nM of [glycerol-1,2,3-^{3}H]AEA was added to the homogenates and incubated for 15 min at 37 °C. The reaction was stopped by the addition of 400 μL of ice-cold $CHCl_3$: MeOH (1:1), samples were vortexed and rapidly centrifuged at 16000 x g for 10 min. at 4 °C. The aqueous phases were collected and the radioactivity was measured for tritium content by liquid scintillation spectroscopy. For AEA uptake assay 0.5 x 10^6 of intact U937 cells were suspended in 500 μL of serum-free medium in silanized glass tubes and preincubated with a screening concentration (10 μM) of the compounds for 20 min at 37 °C. Then, the cells were incubated for 5 min at 37 °C with 100 nM of AEA and a small tracer (0.5 nM) of [ethanolamine-1-^{3}H]AEA was added. The uptake process was stopped by transferring the tubes on ice and by rapid filtration over UniFilter®-96 GF/C filters pre-soaked with PBS supplemented with 0.2% BSA. Cells were washed three times with 100 μL ice-cold PBS supplemented with 1% fatty acid free BSA. After drying, 50 μL MicroScint 20 scintillation cocktail was added to the wells. The radioactivity was measured using a Trilux MicroBeta 1450. hABHD6 and hABHD12 activity was determined using cell homogenates from *h*ABHD6 and *h*ABHD12 stably transfected HEK293 cells. Compounds were pre-incubated with 40 μg of cell homogenate for 30 min at 37 °C in assay buffer (Tris 1 mM, EDTA 10 mM plus 0.1% BSA, pH= 7.6). DMSO was used as vehicle control and WWL70 10 μM or THL 20 μM as positive controls. Then, 10 μM of 2-OG was added and incubated for 5 min at 37 ºC. The reaction was stopped by the addition of 400 μL of ice-cold $CHCl_3$:MeOH (1:1). The samples were vortexed and centrifuged (16000 x g, 10 min, 4 ºC).

Aliquots (200 μL) of the aqueous phase were assayed for tritium content by liquid scintillation spectroscopy. Blank values were recovered from tubes containing no enzyme. Basal 2-OG hydrolysis occurring in non-transfected HEK293 cells was subtracted**.**

4.5. AEA uptake.

AEA uptake inhibition was measured in U937 cells as previously described in detail [36,53]. Briefly, 0.5 x 10^6 U937 cells per sample were incubated with the indicated compounds in RPMI, 37 °C for 15 min. A mixture of [ethanolamine-1-^{3}H]AEA (1 nM) and unlabeled AEA (final 100 nM) was added for 15 min. The uptake process was stopped by rapid filtration and washing with ice-cold PBS 1% BSA fatty acid free. All experiments were performed at least three times in triplicate and data are reported as mean values ± SD.

4.6. Cells line culture and treatment

The human glioma cell line U251MG was obtained from CLS Cell Lines Service GmbH (Eppelheim, Germany) and was cultured in EMEM (Lonza) supplemented with 10% heat-inactivated fetal bovine serum (Euroclone), 1% L-Glutamine, 1% antibiotic mixture, 1% sodium pyruvate, 1% non-essential aminoacids (Euroclone). The human lymphoblastoid lung U937 cell line (used for cell viability assays) was kindly provided by Dr. Michelina Festa (University of Salerno, Italy) and cultured in RPMI 1640 (Invitrogen, San Diego, CA, USA) supplemented with 2 mM L-Glutamine, 50 ng/ml streptomycin, 50 units/ml penicillin, and 10% heat-inactivated fetal bovine serum (Hyclone Laboratories, Logan, UT, USA). All cell cultures were maintained at 37°C in humidified 5 % CO2 atmosphere.

4.7. mAbs and cytofluorimetric analysis

The following mAbs was used for immunostaining and FACS analysis: anti-MICA/B/PE, purchased from R&D Systems (Minneapolis, MN). For the evaluation of MICA/B expression, U251MG cells were plated into p60 tissue culture plates at a density of $2x10^4$ cells/cm^2 and were allowed to grow for 24h. Afterwards, cells were washed with PBS and treated with vehicle or test substance in complete medium respectively and processed as previously described [54]. Following 24h of incubation, immunofluorescence staining was performed. Briefly $2x10^5$ tumor cells were stained with the indicated MICA/B- specific mAbs or the respective isotype controls followed by flow cytometric analysis. Then, cells were stained with the mouse indicated antibodies for 20 minutes at 4°C. Cells were fixed in 1% formaldehyde for data analysis. Sample fluorescence was measured by using the BD FACSVerse™ Flow Cytometer (Becton Dickinson, USA) and flow data were analyzed by using the BD FACSuite software. (Becton Dickinson, San Jose, CA). Data are expressed as logarithmic values of fluorescence intensity.

4.8. Determination of cells viability, MTT assay

Glioma U251MG or lymphoblastoid U937 cells ($4x10^3$/well), were cultured for 24h into 96-well plates before addition of the individual substances at the indicated concentrations and cultured for additional 48 at 37°C. To examine cells' viability it has been used the reduction of tetrazolium salts. The yellow tetrazolium MTT (3-(4, 5-dimethylthiazolyl-2)-2,5-diphenyltetrazolium bromide) is reduced by metabolically active cells, in part by the action of dehydrogenase enzymes, to generate reducing equivalents such as NADH and NADPH. The resulting intracellular purple formazan was solubilized and quantified by spectrophotometric means at 595 nm. All experiments were

performed in triplicate, and the relative cell growth was expressed as a percentage comparison with the untreated control cells.

4.9. Statistical analysis

Statistical analysis was performed in all the experiments shown by using the GraphPad prism 6.0software for Windows (GraphPad software). For each type of assay or phenotypic analysis, data obtained from multiple experiments are calculated as mean ± SD and analyzed for statistical significance using the 2- tailed Student t-test, for independent groups, or ANOVA followed by Bonferroni correction for multiple comparisons. P values less than 0.05 were considered significant. *P<0.05, **P<0.01 and ***P<0.001.

4.10. Calculated ADME properties

Octanol/water partition coefficient (logP), water solubility (logS), Caco-2 and MDCK apparent cell permeability, Lipinski and Jorgensen parameters were calculated using QikProp software within Schrodinger suite [43]. Prior to the ADME properties calculation, the ligands were subjected to torsional sampling conformational search (MCMM) and energy minimization, which were performed using the Macromodel module included in Maestro modeling package [55].

4.11 Homology Modelling

The primary amino acid sequence of the human CB2 receptor was acquired from the SWISS-PROT protein sequence database (code P34972) [56], while the crystal structure of the human CB1 receptor was obtained from the Protein Data Bank (PDB code 5TGZ) [46]. The sequential alignment was performed by means of CLUSTAL W, employing the Blosum series as a matrix,

with a gap open penalty of 10 and a gap extension penalty of 0.05. The TM helices and the extracellular and intracellular loops of the CB2 receptor were created directly from the coordinates of the corresponding amino acids in the CB1 receptor by means of the Modeller program [47]. The presence of a disulfide bridge between C174 and C179 was taken into account, since it seemed to be essential for the receptor function and activity [46]. Starting from this first model, 10 structures were generated through the "very slow MD annealing" refinement method, as implemented in the Modeller software. Based on the DOPE (discrete optimized protein energy) assess method, the best human CB2 receptor model was selected.

4.11 MD simulations

All the simulations were performed using AMBER14 [48]. The simulation protocol, described below, was set up employing as reference the X-ray structure of the human CB1 receptor (PDB code 5TGZ). The CB2 model was embedded into a previously stabilized phospholipid bilayer membrane made up of DPPC molecules [57]. The structure was manually inserted into the phospholipid bilayer membrane in a way that the α helices of the receptor were oriented in parallel to the carbon chains of the DPPC molecules. After that, all the phospholipids within a radius less than 1Å around the receptor were deleted. The system was solvated on the "extracellular" and "intracellular" side with a 20 Å water cap; an explicit solvent model was used for water (TIP3P). Chlorine ions were added as counterions to neutralize the system. Three steps of minimization were carried out prior to MD simulation. In the first stage, the position of the water molecules was minimized just keeping the protein and phospholipids fixed with a constraint of 100 kcal/mol; then, in the second stage, the phospholipids-water system was minimized clamping the whole protein with a constraint of 100 kcal/mol. Finally, in the last stage, a constraint of 10 kcal/mol was applied only on the α carbons of the protein. The whole minimization protocol consisted of 20'000 cycles in

which the first 4’000 were steepest descent (SD) while the last 16’000 conjugate gradient (CG). MD trajectories were run using the previously obtained minimized structure as starting conformation; particle mesh Ewald electrostatics (PME) and periodic boundary conditions were employed in the simulations. A total of 100 ns of MD simulation were run employing a cutoff of 10 Å for the nonbonded interactions and the SHAKE algorithm to keep rigid every bond involving hydrogen. In the first step, 1.5 ns of constant-volume simulation were carried out to increase the temperature from 0 to 300 K. The second step consisted of 98.5 ns of constant pressure simulation, in which the temperature was maintained constant at 300 K by using the Langevin method. In the first 50 ns of the simulation, the α carbons of the receptor and all the heavy atoms of the DPPC molecules were fixed with a harmonic force constant, which decrease during these 50 ns from 10 to 1 kcal/(mol·Å); while in the last 50 ns there were no constraints. The final structure of the CB2 model was obtained as the average of the last 50 ns of MD minimized with the CG method until a convergence of 0.05 kcal/(Å·mol).

4.12 Docking of compound B1-6 and C1-6

Compounds **B1**-**6** and **C1**-**6** were built through Maestro and then energy-minimized using a water environment model (generalized-Born / surface-area model) by means of the Macromodel program [55]. The minimization was performed employing the conjugated gradient method until a convergence value of 0.05 kcal/(Å·mol), the MMFFs as force field and a distance-dependent dielectric constant of 1.0. Compounds were submitted to a conformational search of 1’000 steps with an energy window for saving structures of 10 kJ/mol by means of Macromodel. The algorithm used was the Monte Carlo method; the search was carried out using the same force field and dielectric constant employed for the minimization. All the ligands were docked into the CB1 and CB2 receptors binding pockets by means of AUTODOCK4.2 [58]. The docking sites were defined

superimposing the optimized CB2 model to the template structure (CB1 receptor) and setting the bound AM6538 as the center of a grid of 56, 56 and 50 points, respectively, in the x, *y* and *z* directions. A grid spacing of 0.375 Å and a distance-dependent function of the dielectric constant were used for the energy map calculations. All the compounds were subjected to 200 runs of the AUTODOCK search as previously described [59]. Cluster analysis was carried out on the docked results using an RMS tolerance of 2.0 Å. For each compound, the best docking pose belonging to the best-ranked and most populated cluster was considered. The same docking procedure was applied to dock compounds **B1**-**6** and **C1**-**6** into the catalytic site of the FAAH enzyme (PDB code 3QJ8) [60].

Acknowledgements

This research was supported by grants from University of Pisa, Italy (Progetti di Ricerca di Ateneo, PRA_2017_51). E. Ciaglia was supported by a fellowship from Fondazione Umberto Veronesi (FUV 2018, cod.2153).

Appendix A. Supplementary data

Supplementary data related to this article can be found at

References

[1] V. Di Marzo, Targeting the endocannabinoid system: to enhance or reduce? Nat. Rev. Drug Discov. 7 (2008) 438–455.

[2] B.F. Cravatt, D.K. Giang, S.P. Mayfield, D.L. Boger, R.A. Lerner, N.B. Gilula, Molecular characterization of an enzyme that degrades neuromodulatory fatty-acid amides. Nature 384 (1996) 83–87.

[3] T.P. Dinh, D. Carpenter, F.M. Leslie, T.F. Freund, I. Katona, S.L. Sensi, S. Kathuria, D. Piomelli, Brain monoglyceride lipase participating in endocannabinoid inactivation. Proc. Natl. Acad. Sci. U S A 99 (2002) 10819–10824.

[4] W.R.Marrs, J.L.Blankman, E.A. Horne, A. Thomazeau, Y.H. Lin, J. Coy, A.L. Bodor, G.G. Muccioli, S.S. Hu, G. Woodruff, S. Fung, M. Lafourcade, J.P. Alexander, J.Z. Long, W. Li, C. Xu, T. Möller, K. Mackie, O.J. Manzoni, B.F. Cravatt, N. Stella, The serine hydrolase ABHD6 controls the accumulation and efficacy of 2-AG at cannabinoid receptors. Nat. Neurosci. 13 (2010) 951–957.

[5] J.R. Savinainen, S.M. Saario, J.T. Laitinen, The serine hydrolases MAGL, ABHD6 and ABHD12 as guardians of 2-arachidonoylglycerol signalling through cannabinoid receptors. Acta Physiol. 204 (2012) 267–276.

[6] P. Pacher, G. Kunos, Modulating the endocannabinoid system in human health and disease–successes and failures. FEBS J. 280 (2013) 1918−1943.

[7] T. Jourdan, G. Szanda, A.Z. Rosenberg, J. Tam, B.J. Earley, G. Godlewski, R. Cinar, Z. Liu, J. Liu, C. Ju, P. Pacher, G. Kunos, Overactive cannabinoid 1 receptor in podocytes drives type 2 diabetic nephropathy. Proc. Natl. Acad. Sci. USA 111 (2014) E5420–8.

[8] B. Gatta-Cherifi, D. Cota, New insights on the role of the endocannabinoid system in the regulation of energy balance. Int. J. Obes. (Lond) 40 (2016) 210–219.

[9] W. Mazier, N. Saucisse, B. Gatta-Cherifi, D. Cota, The Endocannabinoid System: Pivotal Orchestrator of Obesity and Metabolic Disease. Trends Endocrinol. Metab. 26 (2015) 524–537.

[10] R.G. Pertwee, Elevating endocannabinoid levels: pharmacological strategies and potential therapeutic applications. Proc. Nutr. Soc. 73 (2014) 96–105.

[11] J.W. Chang, M.J. Niphakis, K.M. Lum, A.B. Cognetta, C. Wang, M.L. Matthews, S. Niessen, M.W. Buczynski, L.H. Parsons, B.F. Cravatt, Highly selective inhibitors of monoacylglycerol lipase bearing a reactive group that is bioisosteric with endocannabinoid substrates. Chem. Biol. 19 (2012) 579–588.

[12] J.R. Clapper, F. Vacondio, A.R. King, A. Duranti, A. Tontini, C. Silva, S. Sanchini, G. Tarzia, M. Mor, D. Piomelli, A second generation of carbamate-based fatty acid amide hydrolase inhibitors with improved activity in vivo. ChemMedChem 4 (2009) 1505–1513.

[13] A. Chicca, C. Arena, C. Manera, Beyond the Direct Activation of Cannabinoid Receptors: New Strategies to Modulate the Endocannabinoid System in CNS-Related Diseases. Recent Pat. CNS Drug Discov. 10 (2016) 122–141.

[14] J.E. Schlosburg, J.L. Blankman, J.Z. Long, D.K. Nomura, B. Pan, S.G. Kinsey, P.T. Nguyen, D. Ramesh, L. Booker, J.J. Burston, E.A. Thomas, D.E. Selley, L.J. Sim-Selley, Q.S. Liu, A.H. Lichtman, B.F. Cravatt, Chronic monoacylglycerol lipase blockade causes functional antagonism of the endocannabinoid system. Nat. Neurosci. 9 (2010) 1113-1119.

[15] W.H. Brown, M.P. Gillum, H.Y. Lee, J.P. Camporez, X.M. Zhang, J.K. Jeong, T.C. Alves, D.M. Erion, B.A. Guigni, M. Kahn, V.T. Samuel, B.F. Cravatt, S. Diano, G.I. Shulman, Fatty acid amide hydrolase ablation promotes ectopic lipid storage and insulin resistance due to centrally mediated hypothyroidism. Proc. Natl. Acad. Sci. U S A. 109 (2012) 14966-4971.

[16] F.F. Hoyer, M. Khoury, H. Slomka, M. Kebschull, R. Lerner, B. Lutz, H. Schott, D. Lütjohann, A. Wojtalla, A. Becker, A. Zimmer, G. Nickeni, Inhibition of endocannabinoid-degrading enzyme fatty acid amide hydrolase increases atherosclerotic plaque vulnerability in mice. J. Mol. Cell. Cardiol. 66 (2014) 126-132.

[17] R. Schwarz , R. Ramer , B. Hinz, Targeting the endocannabinoid system as a potential anticancer approach. Drug Metab. Rev. 50 (2018) 26-53.

[18] J. Fernández-Ruiz, M. Gómez-Ruiz, C. García, M. Hernández, J.A. Ramos, Modeling Neurodegenerative Disorders for Developing Cannabinoid-Based Neuroprotective Therapies. Methods Enzymol. 593 (2017) 175-198.

[19] S. Maione, B. Costa, V. Di Marzo, Endocannabinoids: a unique opportunity to develop multitarget analgesics. Pain 154 Suppl 1 (2013) S87–93.

[20] V. Lucchesi, D.P. Hurst, D.M. Shore, S. Bertini, B.M. Ehrmann, M. Allarà, L. Lawrence, A. Ligresti, F. Minutolo, G. Saccomanni, H. Sharir, M. Macchia, V. Di Marzo, M.E. Abood, P. H. Reggio, C. Manera, CB2-Selective Cannabinoid Receptor Ligands: Synthesis, Pharmacological Evaluation, and Molecular Modeling Investigation of 1,8-Naphthyridin-2(1 H)-one-3-carboxamides. J. Med. Chem. 57 (2014) 8777–8791.

[21] S. Bertini, T. Parkkari, J.R. Savinainen, C. Arena, G. Saccomanni, S. Saguto, A. Ligresti, M. Allarà, A. Bruno, L. Marinelli, V. Di Marzo, E. Novellino, C. Manera, M. Macchia, Synthesis, biological activity and molecular modeling of new biphenylic carboxamides as potent and selective CB2 receptor ligands. Eur. J. Med. Chem. 90 (2015) 526-536.

[22] C. Manera, A.M. Malfitano, T. Parkkari, V. Lucchesi, S. Carpi, S. Fogli, S. Bertini, C. Laezza, A. Ligresti, G. Saccomanni, J.R. Savinainen, E. Ciaglia, S. Pisanti, P. Gazzerro, V. Di Marzo, P. Nieri, M. Macchia, M. Bifulco, New quinolone- and 1,8-naphthyridine-3-carboxamides as selective CB2 receptor agonists with anticancer and immuno-modulatory activity. Eur. J. Med. Chem. 97 (2015) 10–18.

[23] S. Bertini, A. Chicca, C. Arena, S. Chicca, G. Saccomanni, J. Gertsch, C. Manera, M. Macchia, Synthesis and pharmacological evaluation of new biphenylic derivatives as CB2 receptor ligands. Eur J Med Chem. 116 (2016) 252-266.

[24] C. Manera, G. Saccomanni, A.M. Malfitano, S. Bertini, F. Castelli, C. Laezza, A. Ligresti, V. Lucchesi, T. Tuccinardi, F. Rizzolio, M. Bifulco, V. Di Marzo, A. Giordano, M. Macchia, A. Martinelli, Rational design, synthesis and anti-proliferative properties of new CB2 selective

cannabinoid receptor ligands: an investigation of the 1,8-naphthyridin-2(1H)-one scaffold. Eur. J. Med. Chem. 52 (2012) 284–294.

[25] V. Lucchesi, T. Parkkari, J.R. Savinainen, A.M. Malfitano, M. Allarà, S. Bertini, F. Castelli, S. Del Carlo, C. Laezza, A. Ligresti, G. Saccomanni, M. Bifulco, V. Di Marzo, M. Macchia, C. Manera, 1,2-Dihydro-2-oxopyridine-3-carboxamides: the C-5 substituent is responsible for functionality switch at CB2 cannabinoid receptor. Eur. J. Med. Chem. 74 (2014) 524–532.

[26] Q. Zhao, H.G. Chen, C. Qian, X.Z. Chen,. Improved Synthesis of 2-Chloro-3-amino-4-methylpyridine. J. Heterocyclic Chem. 50 (2013) 145-148.

[27] Z. Kibou, N. Cheikh, D. Villemin, N. Choukchou-Braham, B. Mostefa-Kara, M. Benabdallah, Simple and Efficient Procedure for a 2-Pyridones Synthesis under Solvent-Free Conditions. Int. J. Org. Chem. 1 (2011) 242–249.

[28] S. Krawczyk, M. Otto, A. Otto, C. Coburger, M. Krug, M. Seifert, V. Tell, J. Molnár, A. Hilgeroth, Discovery of pyridine-2-ones as novel class of multidrug resistance (MDR) modulators: First structure-activity relationships. Bioorg. Med. Chem. 19 (2011) 6309–6315.

[29] C.A. Lunn, E.P. Reich, J.S. Fine, B. Lavey, J.A. Kozlowski, R.W. Hipkin, D.J. Lundell, L. Bober, Biology and therapeutic potential of cannabinoid CB2 receptor inverse agonists. Br. J. Pharmacol. 153 (2008) 226-239.

[30] S. Marino, AI. Idris, Emerging therapeutic targets in cancer induced bone disease: A focus on the peripheral type 2 cannabinoid receptor. Pharmacol. Res. 119 (2017) 391-403.

[31] D. Bolognini, M.G. Cascio, D. Parolaro, R.G. Pertwee, AM630 behaves as a protean ligand at the human cannabinoid CB2 receptor. Br. J. Pharmacol. 165 (2012) 2561-2574.

[32] P. Marini, M.G. Cascio, A. King, R.G. Pertwee, R.A. Ross, Characterization of cannabinoid receptor ligands in tissues natively expressing cannabinoid CB2 receptors. Br. J. Pharmacol. 169 (2013) 887-899.

[33] A. Dhopeshwarkar, K. Mackie, Functional Selectivity of CB2 Cannabinoid Receptor Ligands at a Canonical and Noncanonical Pathway, J. Pharmacol. Exp. Ther. 358 (2016) 342-351.

[34] A. Chicca, J. Marazzi, S. Nicolussi, J. Gertsch, Evidence for bidirectional endocannabinoid transport across cell membranes. J. Biol. Chem. 287 (2012) 34660-34682.

[35] S. Nicolussi, J. Gertsch, Endocannabinoid transport revisited. Vitam. Horm. 98 (2015)441-485.

[36] A. Chicca, S. Nicolussi, R. Bartholomäus, M. Blunder, A.A. Rey, V. Petrucci, I. del Carmen Reynoso-Moreno, J.M. Viveros-Paredes, M. Dalghi Gens, B. Lutz, H.B. Schiöth, M. Soeberdt, C. Abels, R-P. Charles, K-H. Altmann, J. Gertsch, Chemical probes to potently and selectively inhibit endocannabinoid cellular reuptake. Proc. Natl. Acad. Sci. U S A. 114 (2017) E5006-E5015.

[37] A. Chicca, D. Caprioglio, A. Minassi, V. Petrucci, G. Appendino, O. Taglialatela-Scafati, J. Gertsch, Functionalization of β-caryophyllene generates novel polypharmacology in the endocannabinoid system. ACS Chem. Biol. 9 (2014) 1499-1507.

[38] S. Ghosh, S.G. Kinsey, Q.S. Liu, L. Hruba, L.R. McMahon, T.W. Grim, C.R. Merritt, L.E. Wise, R.A. Abdullah, D.E. Selley, L.J. Sim-Selley, B.F. Cravatt, A.H. Lichtman, Full fatty acid amide hydrolase inhibition combined with partial monoacylglycerol lipase inhibition: augmented and sustained antinociceptive effects with reduced cannabimimetic side effects in mice. J. Pharmacol. Exp. Ther.354 (2015) 111-120.

[39] S.G. Kinsey, L.E. Wise, D. Ramesh, R. Abdullah, D.E. Selley, B.F. Cravatt, A.H. Lichtman, Repeated low-dose administration of the monoacylglycerol lipase inhibitor JZL184 retains cannabinoid receptor type 1-mediated antinociceptive and gastroprotective effects. J. Pharmacol. Exp. Ther. 345 (2013) 492-501.

[40] R.J. McKallip, C. Lombard, M. Fisher, B. R. Martin, S. Ryu, S. Grant, P.S. Nagarkatti, M. Nagarkatti, Targeting CB2 cannabinoid receptors as a novel therapy to treat malignant lymphoblastic disease. Blood. 100 (2002) 627-634.

[41] M. Alberich Jordà, N. Rayman, M. Tas, S.E. Verbakel, N. Battista, K. van Lom, B. Löwenberg, M. Maccarrone, R. Delwel, The peripheral cannabinoid receptor Cb2, frequently expressed on AML blasts, either induces a neutrophilic differentiation block or confers abnormal migration properties in a ligand-dependent manner. Blood. 104 (2004) 526-534.

[42] E. Ciaglia, G. Torelli, S. Pisanti,; P. Picardi, A. D'Alessandro, C. Laezza, A.M. Malfitano,; Fiore, D.; A.C. Pagano Zottola,; M.C. Proto,; G. Catapano, P. Gazzerro, M. Bifulco, Cannabinoid receptor CB1 regulates STAT3 activity and its expression dictates the responsiveness to SR141716 treatment in human glioma patients' cells. Oncotarget. 6 (2015) 15464-15481.

[43] QikProp, Version 4.7, Schrödinger, Inc., New York, 2016.

[44] J.D. Irvine, L. Takahashi, K. Lockhart, J. Cheong, J.W. Tolan, H.E. Selick, J.R. Grove, MDCK (Madin-Darby canine kidney) cells: A tool for membrane permeability screening. J. Pharm. Sci. 88 (1999) 28-33.

[45] A.M. Malfitano, C. Laezza, S. Bertini, D. Marasco, T. Tuccinardi, M. Bifulco, C. Manera. Immunomodulatory properties of 1,2-dihydro-4-hydroxy-2-oxo-1,8-naphthyridine-3-carboxamide derivative VL15. Biochimie. 135 (2017) 173-180.

[46] T. Hua, K. Vemuri, M. Pu, L. Qu, G.W. Han, Y. Wu, S. Zhao, W. Shui, S. Li, A. Korde, R.B. Laprairie, E.L. Stahl, J.H. Ho, N. Zvonok, H. Zhou, I. Kufareva, B. Wu, Q. Zhao, M.A. Hanson, L.M. Bohn,; A. Makriyannis, R.C. Stevens, Z.J. Liu, Crystal Structure of the Human Cannabinoid Receptor CB1. Cell. 167 (2016) 750-762.

[47] A. Fiser, R.K. Do, A. Sali, Modeling of loops in protein structures. Protein Sci. 9 (2000) 1753-1773.

[48] D.A. Case, J.T. Berryman, R.M. Betz, D.S. Cerutti, T.E. III Cheatham, T.A. Darden, R.E. Duke, T.J. Giese, H. Gohlke, A. W. Goetz, N. Homeyer, S. Izadi, P. Janowski, J. Kaus, A. Kovalenko, T.S. Lee, S. LeGrand, P. Li, T. Luchko, R. Luo, B. Madej, K.M. Merz, G. Monard,

P. Needham, H. Nguyen, H.T. Nguyen, I. Omelyan, A. Onufriev, D.R. Roe, A. Roitberg, R. Salomon-Ferrer, C.L. Simmerling, W. Smith, J. Swails, R.C. Walker, J. Wang, R.M. Wolf, X. Wu, D.M. York, P.A. Kollman, AMBER version 14; University of California: San Francisco, CA, 2015.

[49] A.D. Favia, D. Habrant, R. Scarpelli, M. Migliore, C. Albani, S.M. Bertozzi, M. Dionisi, G. Tarozzo, D. Piomelli, A. Cavalli, M. De Vivo, Identification and characterization of carprofen as a multitarget fatty acid amide hydrolase/cyclooxygenase inhibitor. J Med. Chem. 55 (2012) 8807-8826.

[50] S. Gouveia-Figueira, J. Karlsson, A. Deplano, S. Hashemian, M. Svensson, M. Fredriksson Sundbom, C. Congiu, V. Onnis, C.J. Fowler, Characterisation of (R)-2-(2-Fluorobiphenyl-4-yl)-N-(3-Methylpyridin-2- yl)Propanamide as a dual fatty acid amide hydrolase: Cyclooxygenase inhibitor. PLoS One 10 (2015) e0139212.

[51] M.S. Crowe, E. Leishman, M.L. Banks, R. Gujjar, A. Mahadevan, H.B. Bradshaw, S.G. Kinsey, Combined inhibition of monoacylglycerol lipase and cyclooxygenases synergistically reduces neuropathic pain in mice. Br. J. Pharmacol. 172 (2015) 1700-1712.

[52] V. Petrucci, A. Chicca, S. Glasmacher, J. Paloczi, Z. Cao, P. Pacher, J Gertsch.. Pepcan-12 (RVD-hemopressin) is a CB2 receptor positive allosteric modulator constitutively secreted by adrenals and in liver upon tissue damage. Sci. Rep. 7 (2017) 9560.

[53] S. Nicolussi, A. Chicca, M. Rau, S. Rihs, M. Soeberdt, C. Abels, J. Gertsch, Correlating FAAH and anandamide cellular uptake inhibition using N-alkylcarbamate inhibitors: from ultrapotent to hyperpotent. Biochem. Pharmacol. 92 (2014) 669-689.

[54] A.M. Malfitano, C. Laezza, G. Saccomanni, T. Tuccinardi, C. Manera, A. Martinelli, E. Ciaglia, S. Pisanti, M. Vitale, P. Gazzerro, M. Bifulco, Immune-modulation and properties of absorption and blood brain barrier permeability of 1,8-naphthyridine derivatives. J. Neuroimmune Pharmacol. 8 (2013) 1077-1086.

[55] Macromodel, Version 11.1, Schrödinger, Inc., New York, 2016.

[56] E. Gasteiger, A. Gattiker, C. Hoogland, I. Ivanyi, R.D. Appel, A. Bairoch. ExPASy: The proteomics server for in-depth protein knowledge and analysis. Nucleic Acids Res. 31 (2003) 3784-3788.

[57] T. Tuccinardi, S. Schenone, F. Bondavalli, C. Brullo, O. Bruno, L. Mosti, A.T. Zizzari, C. Tintori, F. Manetti, O. Ciampi, M.L. Trincavelli, C. Martini, A. Martinelli, M. Botta. Substituted pyrazolo[3,4-b]pyridines as potent A1 adenosine antagonists: synthesis, biological evaluation, and development of an A1 bovine receptor model. ChemMedChem. 3 (2008) 898-913.

[58] G.M. Morris, R. Huey, W. Lindstrom, M.F. Sanner, R.K. Belew, D.S. Goodsell, A.J. Olson, J. Comp. Chem. 30 (2009) 2785-2791.

[59] F. Dal Piaz, M.B. Vera Saltos, S. Franceschelli, G. Forte, S. Marzocco, T. Tuccinardi, G. Poli, S. Nejad Ebrahimi, M. Hamburger, N. De Tommasi, A. Braca, J. Nat. Prod. 79 (2016) 2681-2692.

[60] X. Min, S.T. Thibault, A.C. Porter, D.J. Gustin, T.J. Carlson, H. Xu, M. Lindstrom, G. Xu, C. Uyeda, Z. Ma, Y. Li, F. Kayser, N.P. Walker, Z. Wang, Proc. Natl. Acad. Sci. U S A 108 (2011) 7379-7384.